NASA TECHNICAL REPORT

NASA TR R-177

NASA TR R-177

THE EFFECT OF A RING CURRENT ON THE BOUNDARY OF THE GEOMAGNETIC FIELD IN A STEADY SOLAR WIND

by John R. Spreiter and Alberta Y. Alksne

Ames Research Center
Moffett Field, Calif.

NATIONAL AERONAUTICS AND SPACE ADMINISTRATION • WASHINGTON, D. C. • DECEMBER 1963

THE EFFECT OF A RING CURRENT ON THE BOUNDARY OF THE GEOMAGNETIC FIELD IN A STEADY SOLAR WIND

By John R. Spreiter and Alberta Y. Alksne

Ames Research Center
Moffett Field, Calif.

NATIONAL AERONAUTICS AND SPACE ADMINISTRATION

For sale by the Office of Technical Services, Department of Commerce,
Washington, D.C. 20230 -- Price $1.25

NATIONAL AERONAUTICS AND SPACE ADMINISTRATION

TECHNICAL REPORT R-177

THE EFFECT OF A RING CURRENT ON THE BOUNDARY OF THE GEOMAGNETIC FIELD IN A STEADY SOLAR WIND

By John R. Spreiter and Alberta Y. Alksne

SUMMARY

Approximate solutions are given for the shape of the boundary separating a steady neutral stream of ionized solar corpuscles from the combined magnetic fields of a three-dimensional dipole and an equatorial ring current. Results are presented for the traces of the boundary in the geomagnetic meridian plane containing the sun-earth line for several orientations of the latter relative to the dipole axis, and for the trace of the boundary in the geomagnetic equatorial plane for the case in which the dipole axis is normal to the sun-earth line. It is found that the presence of a ring current having values for the diameter and strength of the order proposed to explain the magnetometer data from Pioneer I and Pioneer V has the effect of greatly increasing the size, as well as altering the form, of the region within which the geomagnetic field is confined.

INTRODUCTION

The present paper reports the results of an extension of the theoretical study reported in references 1, 2, and 3 in which approximate results are determined for the traces, in the geomagnetic equatorial plane and in the geomagnetic meridian plane containing the sun-earth line, of the cavity carved out of a steady neutral ionized solar corpuscular stream by interaction with a magnetic dipole representing the geomagnetic field. The novel feature of this extension is the inclusion of the effect of an equatorial ring current having properties similar to those of the model proposed by Smith, Coleman, Judge, and Sonett in reference 4 to represent the magnetometer data from Pioneer V and Explorer VI. These properties are that there exists, during quiet times, a westward flowing current of about 5×10^6 amperes distributed over a large volume having the form of a toroidal ring 3 earth radii in cross-sectional radius with its center line situated in the geomagnetic equatorial plane at a distance of approximately 8 to 10 earth radii. The magnetic moment of such a current system is of the same sign and order of magnitude as that of the main dipole field. Although the concept of a ring current is of long standing in the explanation of the decrease of the horizontal component of the magnetic field in the main phase of a magnetic

storm, and values for the strength and radius similar to those stated above have also been deduced recently from cosmic-ray data by Kellogg and Winckler (ref. 5), magnetometer and other data from more recent space experiments with Explorer X (ref. 6) and Explorer XII (ref. 7) have failed to detect the presence of such substantial ring-current effects. As a result, the entire subject of the properties and even the existence of a significant ring current must be regarded as an open question at the present time.

It is evident that the presence of a ring current having a magnetic moment comparable to that of the permanent magnetic field of the earth should have the effect of greatly increasing the size, as well as altering the form, of the cavity. It is the purpose of this paper to present the results of a number of calculations undertaken to determine in a more quantitative manner the nature of the effects of such a ring current. A preliminary account of the present investigation including plots of the results for the case in which the dipole axis is normal to the direction of the incident stream has been given in reference 8. Those results are presented in greater detail in the present paper. Also presented are additional results for the traces of the boundary in the above specified meridian plane for other orientations of the dipole axis relative to the stream direction.

It should be recognized that the concept of a toroidal ring current with protons and electrons circulating round the geomagnetic axis at different speeds, although simple and of long standing, is, at best, not particularly precise. Singer has proposed a different concept in reference 9 in which the observed magnetic variations and the associated ring current are explained in terms of the spiraling and drifting motion of trapped particles similar to those discovered shortly thereafter by satellite experiments by Van Allen and his colleagues (see, e.g., ref. 10). As is now familiar, the trapped particles spiral rapidly to and fro along the local magnetic lines between mirror points in the northern and southern hemispheres. At the same time the trapped particles drift round the earth, the protons to the west, the electrons to the east, thus setting up a westward electric current. This current is identified with the ring current. There is, in addition, a diamagnetic effect produced by the gyration of the particles about the line of force. Superposition of these two effects gives the total magnetic influence, although Singer states in reference 11 that under certain conditions, the diamagnetic effects are not important.

It is assumed in the present investigation that the simple ring current model proposed by Smith, Coleman, Judge, and Sonett in reference 4 can be used to obtain an adequate representation of the basic geomagnetic field. It should be recognized that the values indicated for the strength and position of the ring current may be at considerable variance with those of the equivalent diamagnetic ring current which could also be used to represent the measured field, but which would be more consistent with the concept of the magnetic field arising from the motion of trapped particles. It is not necessary, however, for the determination of the terminal shape of the geomagnetic field to duplicate the properties of the ring current in all details. It is important, though, that a consistent system be employed so that the approximations introduced in proceeding from the measured values to an equivalent current system are removed when the process is repeated in reverse order to calculate the magnetic field. This has been done in the

present analysis, and all results presented herein are based on the consistent use of the model and associated numerical values proposed by Smith, Coleman, Judge, and Sonett. The only deviation is that the ring current of finite cross section is replaced by an idealized one of infinitesimal cross section. This change simplifies the computations considerably and should lead to little difference in the results, provided the boundary of the cavity is farther than about 2 or 3 earth radii from the idealized ring current.

PRINCIPAL SYMBOLS

a	radius of ring current, cm (see fig. 1)
a_e	radius of earth, cm
$\underset{\sim}{B}$	total magnetic field, gauss
$\underset{\sim}{B}'$	magnetic field due to currents in boundary, gauss
B_{p_o}	intensity of geomagnetic field at equator ≈ 0.312 gauss
B_s	intensity of field at the boundary, gauss
$\bar{B}_\theta$	$B_\theta r_o^3/M_p$ (see eq. (9))
$\bar{B}_\rho$	$B_r r_o^3/M_p$ (see eq. (9))
E	complete elliptic integral of the second kind
i	current, e.m.u.
K	complete elliptic integral of the first kind
k	modulus of elliptic integrals
M_p	dipole moment of earth = $a_e^3 B_{p_o}$
M_i	dipole moment of ring current = $\pi a^2 i$
m	mass of proton $\approx 1.67 \times 10^{-24}$ gm
n	number of protons per cm^3
$\hat{n}$	unit vector in the direction of the outward normal to the boundary
r, φ, θ	spherical coordinates (see fig. 1)
$\hat{r}$	unit vector in radial direction

r_o	unit of length defined by equation (8), cm
v	velocity of plasma, cm/sec
x, y, z	rectangular coordinates (geomagnetic, see fig. 1)
x', y', z'	rectangular coordinates (geographic)
α	a/r_o (see eq. (9))
$\hat{\theta}$	unit vector in direction of increasing θ
λ	angle between direction of undisturbed plasma stream and the geomagnetic equatorial plane (see fig. 1)
μ	M_i/M_p
ρ	r/r_o
ψ	angle between direction of undisturbed plasma stream and the outward normal to the boundary (see fig. 1)

Subscripts

F	front
i	pertaining to ring current
L	lower
N	neutral point
p	pertaining to permanent, or dipole, field
R	rear
U	upper
θ	component in the direction of increasing θ
ρ	component in the direction of increasing ρ

FUNDAMENTAL ASSUMPTIONS AND EQUATIONS

The basic concepts of the present study are classical and stem from a long series of investigations by Chapman, Ferraro, Dungey, and others (see refs. 12 and

13 for a résumé) undertaken to explain the connection between solar flares and geomagnetic storms. The fundamental assumption is that there exists a rarefied neutral ionized corpuscular stream, the solar wind, consisting principally of protons and electrons in equal numbers, which flows past the earth at hypersonic speeds. The particles are presumed to be of solar origin, and to be of uniform velocity in the undisturbed incident stream. The direction of the incident stream will be referred to for convenience of discussion as though it were coming directly from the sun. It should be understood, however, that the direction of the sun is actually immaterial in the analysis, and that only the direction of the undisturbed incident stream relative to the dipole axis is significant. Interaction between the solar wind and the permanent geomagnetic field is such that a cavity, bounded by a thin current sheath, is carved out of the stream. The solar wind is thus confined to the exterior, and the geomagnetic field to the interior, of the cavity. The latter region, dominated by the geomagnetic field, is now generally referred to as the magnetosphere.

The particles of the solar wind are considered to move in straight lines up to the boundary of the cavity where they are, in effect, specularly reflected and returned to the stream with a direction of motion different from that which they possessed in the incident stream. By this process they exert a pressure $2mnv^2 \cos^2 \psi$ on any element of the boundary for which $\cos \psi \leq 0$. The quantities m, n, and v represent the mass, number density, and velocity of the protons in the undisturbed incident stream, and ψ represents the angle between the free-stream velocity vector and an outward normal to the surface. An element of the surface that fails to comply with the condition that $\cos \psi \leq 0$ is shielded from the stream and experiences no pressure.

Dungey (ref. 13) has investigated the conditions that prevail in the current sheath bounding the cavity and has shown that the particle pressure is balanced by the magnetic pressure $B_s^2/8\pi$ where B_s is the total (tangential) magnetic field at the surface of the cavity. These considerations lead to the following relation which must be satisfied at the boundary:

$$B_s^2/8\pi = 2mnv^2 \cos^2 \psi \tag{1}$$

with m, n, and v expressed in c.g.s. units and B_s expressed in gauss.

The total magnetic field $\underset{\sim}{B}$ in the cavity is considered to be the sum of the permanent magnetic field $\underset{\sim}{B}_p$ of terrestrial origin, the field $\underset{\sim}{B}_i$ induced by the ring current, and the field $\underset{\sim}{B}'$ due to the currents in the boundary. It is a fundamental assumption of the theory that the total field inside the cavity satisfy the magnetic field equations for a vacuum

$$\operatorname{div} \underset{\sim}{B} = 0 , \qquad \operatorname{curl} \underset{\sim}{B} = 0 \tag{2}$$

together with the boundary conditions that the normal component of $\underset{\sim}{B}$ vanish and the tangential component of $\underset{\sim}{B}$ be given by equation (1) at the surface of the cavity. It is also necessary that the solution possess the appropriate singularities in the cavity that are required to represent $\underset{\sim}{B}_p$ and $\underset{\sim}{B}_i$. The first of these will be considered to be represented by a single magnetic dipole, thus

$$\underset{\sim}{B}_p = \hat{\theta}B_{p_\theta} + \hat{r}B_{p_r} = -(M_p/r^3)(\hat{\theta} \sin \theta + \hat{r}2 \cos \theta) \tag{3}$$

where the coordinate system is fixed with respect to the dipole as illustrated in figure 1, $\hat{\theta}$ and $\hat{r}$ are unit vectors in the direction of increasing θ and r, and the magnetic moment of the dipole is given by $M_p = a_e{}^3B_{p_o}$ where a_e represents the radius of the earth (6.37×10^8 cm) and B_{p_o} represents the intensity of the geomagnetic field at the magnetic equator (0.312 gauss). The second is given by (see, for instance, ref. 14)

$$\underset{\sim}{B}_i = \hat{\theta}B_{i_\theta} + \hat{r}B_{i_r} = \frac{2M_i}{\pi a^2(a^2 + r^2 + 2ar \sin \theta)^{1/2}} \left[\frac{\hat{\theta}}{\sin \theta} \left(K - \frac{a^2 + r^2 - 2a^2 \sin^2 \theta}{a^2 + r^2 - 2ar \sin \theta} E \right) \right.$$

$$\left. - \hat{r} \left(\frac{2a^2 \cos \theta}{a^2 + r^2 - 2ar \sin \theta} E \right) \right] \tag{4}$$

where E and K are complete elliptic integrals having the modulus

$$k = \left(\frac{4ar \sin \theta}{a^2 + r^2 + 2ar \sin \theta} \right)^{1/2} \tag{5}$$

and a and M_i represent the radius and magnetic moment of the ring current. The latter is defined by

$$M_i = \pi a^2 i \tag{6}$$

where i represents the current measured in e.m.u. and considered positive when flowing westward around the earth. One e.m.u. of current is equal to 10 amperes.

It is a property of the above equations that $\underset{\sim}{B}$ cannot vanish over any region of finite extent in the interior of the cavity. It follows that the boundary of the cavity must be of such form that $\cos \psi \leq 0$ everywhere, with zero values occurring only at isolated points. This condition together with the above equations suffices to specify completely the form for the boundary of the cavity and the properties of the magnetic field contained therein.

DERIVATION OF AN APPROXIMATE DIFFERENTIAL EQUATION FOR THE COORDINATES OF THE BOUNDARY OF THE CAVITY

Although the simplified physical model described above leads to a completely defined mathematical problem, the exact solution has still to be determined, even for the case of the dipole alone. The present analysis, therefore, is based on the use of the approximation introduced and commented upon recently by Beard (ref. 15), Ferraro (ref. 16), and Davis and Beard (ref. 17). It is judged on the basis of previous experience with the case of the dipole alone that results obtained in this way display nearly all the essential features of the exact

solution, although the coordinates of the boundary may be in error by a few percent one way or the other at various points. This statement is based principally on comparisons of exact and approximate solutions for the analogous problem in two dimensions given by Hurley (ref. 18), and by Spreiter and Briggs (refs. 1 and 2).

The essential concept that leads to the simplification achieved by Beard is that of relinquishing the condition that the normal component of $\underset{\sim}{B}$ vanish at the boundary of the cavity and replacing it by the approximate relation that B_s be equal to twice the tangential component of the permanent magnetic field $\underset{\sim}{B}_p$ at the same point. Ferraro subsequently suggested that it would be better to replace the factor 2 by 2f where f is a constant, the value for which is to be determined at the end of the calculation by matching conditions at some particularly significant point. These concepts have been carried over to the present study, for which they lead to the approximate relation

$$B_s^2 = 4f^2[\hat{n} \times (\underset{\sim}{B}_p + \underset{\sim}{B}_i)]^2 \tag{7}$$

where $\hat{n}$ is a unit vector in the direction of the outward normal to the surface of the cavity. Ferraro proceeds to present a simple illustrative two-dimensional example involving flow past a current bearing wire, and shows that a reasonable procedure for the estimation of f leads to the value 0.68 for that particular case. It was subsequently shown elsewhere that the value for f increases to about 0.91 when flow past a two-dimensional dipole is considered (refs. 1, 2, and 18), and to 1.29 for a three-dimensional dipole immersed in a stationary plasma (ref. 19). Since the linear dimensions of the cavity are proportional to the first power of f for the wire problem, to the square root of f for the two-dimensional problem, and to the cube root of f for the three-dimensional dipole problem, the use of these values instead of unity leads to reductions of all dimensions of the cavities around the wire and the two-dimensional dipole by 32 percent and 5 percent, respectively, and to an increase of the dimensions of the cavity around the three-dimensional dipole by 9 percent. Corresponding results have not been determined for the present case, however, and f is equated to unity in all numerical examples presented herein.

It should be observed that the expression for B_s given by equation (7) is as indicated by Davis and Beard in reference 17 and, due to the correction of an error, differs from that given previously in references 1, 2, 8, 15, and elsewhere. As noted by Davis and Beard, the difference disappears when attention is confined to the meridian plane containing the sun-earth line, and to the equatorial plane for the case in which the dipole axis is normal to the direction of the incident stream. Solutions given previously for these planes are thus correct in spite of their derivation, but results for the coordinates of the remainder of the surface must be recalculated in order to be consistent with equation (7).

Equations (3) through (7) suffice to provide a relation expressing the left-hand side of equation (1) in terms of the coordinates of the surface of the cavity, the dipole moment of the permanent magnetic field, and the radius and magnetic moment of the ring current. The variable part, cos ψ, of the right side of equation (1) can also be expressed in terms of the coordinates of the surface.

Combining these relations leads to a partial differential equation for the radial coordinate r of the surface expressed as a function of the angular coordinates θ and φ. The equation is lengthy, however, and it is desirable before displaying it to achieve a certain economy resulting from a reduction in the number of parameters by introducing the following quantity for the unit of length

$$r_o = \left(\frac{4f^2 M_p^2}{16\pi m n v^2}\right)^{1/6} = a_e \left(\frac{4f^2 B_{p_o}^2}{16\pi m n v^2}\right)^{1/6} \tag{8}$$

together with the following ratios

$$\rho = r/r_o, \quad \alpha = a/r_o, \quad \mu = M_i/M_p, \quad \bar{B}_\theta = B_\theta r_o^3/M_p, \quad \bar{B}_\rho = B_r r_o^3/M_p \tag{9}$$

The governing equation can thus be written

$$\left\{\frac{\left(B_{p_\rho} + B_{i_\rho}\right)^2 + \left(B_{p_\theta} + B_{i_\theta}\right)^2}{\rho^2 \sin^2\theta}\left(\frac{\partial\rho}{\partial\varphi}\right)^2 + \left[\left(B_{p_\theta} + B_{i_\theta}\right) + \frac{\left(B_{p_\rho} + B_{i_\rho}\right)}{\rho}\frac{\partial\rho}{\partial\theta}\right]^2\right\}$$

$$= \left[\sin\varphi \sin\theta \cos\lambda - \cos\theta \sin\lambda - \frac{\partial\rho}{\rho\,\partial\theta}(\sin\varphi \cos\theta \cos\lambda + \sin\theta \sin\lambda)\right.$$

$$\left. - \frac{\partial\rho}{\rho \sin\theta\,\partial\varphi}\cos\varphi \cos\lambda\right]^2 \equiv \cos^2\psi \tag{10}$$

where

$$\bar{B}_{p_\theta} = -\sin\theta/\rho^3, \qquad \bar{B}_{p_\rho} = -2\cos\theta/\rho^3 \tag{11}$$

$$\left.\begin{aligned} \bar{B}_{i_\theta} &= \frac{2\mu}{\pi\alpha^2(\alpha^2 + \rho^2 + 2\alpha\rho\sin\theta)^{1/2}\sin\theta}\left(K - \frac{\alpha^2 + \rho^2 - 2\alpha^2\sin^2\theta}{\alpha^2 + \rho^2 - 2\alpha\rho\sin\theta}E\right) \\ \bar{B}_{i_\rho} &= \frac{-4\mu a^2 E\cos\theta}{\pi\alpha^2(\alpha^2 + \rho^2 + 2\alpha\rho\sin\theta)^{1/2}(\alpha^2 + \rho^2 - 2\alpha\rho\sin\theta)} \end{aligned}\right\} \tag{12}$$

where E and K are complete elliptic integrals having the modulus

$$k = \left(\frac{4\alpha\rho\sin\theta}{\alpha^2 + \rho^2 + 2\alpha\rho\sin\theta}\right)^{1/2} \tag{13}$$

where λ denotes the angle in the yz plane between the direction of the incident stream and the normal to the axis of the dipole as shown in figure 1. The quantity r_o has physical significance as the geocentric distance along the sun-earth line to the boundary of the geomagnetic field for the case $i = 0$, $\lambda = 0$. The dimensionless radius vector ρ defining the form of the boundary of the cavity as a function of θ and φ thus depends on the parameters μ and λ. The determination of the size of the cavity for any particular combination of density and velocity of the incident stream requires, in addition, the calculation of the unit of length r_o.

When $\partial\rho/\partial\varphi = 0$, as it is in the meridian plane containing the sun-earth line, the first term on the left side of equation (10) is zero and it is possible to take the square root of both sides of the equation. In so doing, it is important that the $\pm$ sign is used in such a way that both sides of the equation are of the same sign. The term within the square bracket on the right side is equal to $-\cos\psi$ and is therefore positive. The term within the square bracket on the left side may be of either sign, however, depending upon whether the tangential component of $\underset{\sim}{B}_p + \underset{\sim}{B}_i$ is oriented in the direction of increasing or decreasing θ. Both cases occur in the desired solution, since all field lines on the surface of the cavity diverge from and converge to a pair of isolated neutral points. These points are of additional interest because the magnetic field lines turn abruptly there and extend to the earth. The intersections of these lines and the earth's surface define a pair of isolated points in the vicinity of the geomagnetic poles through which pass all of the field lines that lie in and define the boundary of the cavity. These points are of special significance because they locate the geographical areas into which can precipitate charged particles initially trapped in the vicinity of the boundary of the geomagnetic field.

SOLUTION FOR THE MERIDIAN PLANE CONTAINING DIPOLE AXIS AND SUN-EARTH LINE

The solution of equations (10) through (13) is unquestionably complex, but can be simplified considerably if attention is confined to determining the trace of the boundary of the cavity in the meridian plane containing the dipole axis and the sun-earth line, that is, the plane along which $\varphi = \pm\pi/2$. Along this plane $\partial\rho/\partial\varphi$ vanishes by reason of symmetry, and the governing equation reduces to an ordinary differential equation in which $\partial\rho/\partial\theta$ can be replaced by $d\rho/d\theta$. This equation can be solved for $d\rho/d\theta$ to yield

$$\frac{d\rho}{d\theta} = \rho \left\{ \frac{(\sin\theta)[\cos\lambda \sin(\pm\pi/2) \mp (1/\rho^3)] - \cos\theta \sin\lambda \pm \bar{B}_{i_\theta}}{(\cos\theta)[\cos\lambda \sin(\pm\pi/2) \pm (2/\rho^3)] + \sin\theta \sin\lambda \mp \bar{B}_{i_\rho}} \right\} \qquad (14)$$

where the sense of the plus and minus signs has been retained to be the same as in the preceding equations by writing $\sin(\pm\pi/2)$ for $\sin(\varphi = \pm\pi/2) = \pm 1$ in the right-hand member. It is convenient to consider the two rearranged families of solutions associated with the following equation, equivalent to equation (14)

$$\frac{d\rho}{d\theta} = \rho \left\{ \frac{\sin [\theta - \lambda \sin (\pm\pi/2)] \mp (\sin \theta)/\rho^3 \pm \bar{B}_{i_\theta}}{\cos [\theta - \lambda \sin (\pm\pi/2)] \pm 2(\cos \theta)/\rho^3 \mp \bar{B}_{i_\rho}} \right\} \tag{15}$$

If the intensity of the ring current is zero, $\bar{B}_{i_\theta} = \bar{B}_{i_\rho} = 0$, and the solution for any λ can be determined in analytic form as shown in references 1 and 2. It was found that the upper signs give a result appropriate for the nose or front portion of the boundary, and the lower signs a result appropriate for the rear portion. The results become particularly simple for the case in which the incident stream is normal to the dipole axis so that $\lambda = 0$. In this case the coordinates of the front portion of the boundary are given by

$$\rho = 1 \tag{16}$$

and those of the rear portion by

$$\rho \cos \theta = \pm \frac{3}{2^{2/3}} \frac{\rho^3}{\rho^3 + 1} \approx \pm 1.89 \frac{\rho^3}{\rho^3 + 1} \tag{17}$$

The curves representing the front and rear portions of the boundary join together at an angle θ_N given for the upper half plane by

$$\theta_{N_U} = \cos^{-1} \left(\frac{3}{4}\right)\left(2^{1/3}\right) = \frac{1}{3} \text{ radian} \approx 19.1^\circ \tag{18}$$

This point and the corresponding point in the lower half plane are of particular physical significance because they correspond to the neutral points described in the preceding section.

The greater complexity inherent in equation (15) when the intensity of the ring current is not zero precludes solution in analytic form, but results can still be obtained by standard numerical techniques. There remains, however, the discussion of the choice of the appropriate integration constant or, what is equivalent, the appropriate combination of ρ and θ to use as starting values in the numerical integration. The appropriate choice for the starting values required to define uniquely the desired solution that satisfies all the auxiliary conditions of the problem is not immediately evident, since there is no point on the boundary for which the coordinates ρ and θ are known from a priori considerations. Examination of the properties of the integral curves for equation (15) discloses, however, that only one of the many alternative solutions satisfies the condition that the cavity extends a finite distance from the ring current in the direction of the sun, and that the lateral dimensions increase steadily with distance downstream from the apex so that $\cos \psi \leq 0$ at all points.

This statement is illustrated most readily by consideration of a case in which $\lambda = 0$. Plots of the integral curves for the upper half plane are shown in

figure 2 for the case in which $\alpha = 1$ and $\mu = 1$. The corresponding curves for the lower half plane need not be considered for the case of $\lambda = 0$, since the form of the hollow is symmetric about the sun-earth line. Although the integral curves shown in figure 2 are for a particular pair of values for α and μ, they are typical because integral curves for other values of these parameters are qualitatively similar. Also indicated on these plots are the positions of the three singular points of equation (15) that are in or adjacent to the upper half plane. These points are designated according to their general location by the terms, front S_F, rear S_R, and upper S_U. Their coordinates are determined by the condition that the numerator and denominator of the right-hand members of equation (15) vanish simultaneously. Their significance derives from the fact that the only integral curves that satisfy all the stated requirements for an acceptable solution pass through a singular point. Thus, the only integral curve that intersects the sun-earth line at a finite and nonvanishing distance upstream from the ring current is that shown on part (a) of figure 2, which passes through S_F. This curve is, therefore, the only one that can represent the trace of the cavity boundary in the vicinity of the apex. This curve cannot represent the trace of the boundary for $\varphi = -\pi/2$, however, since it turns away from the direction of the corpuscular stream over the pole and fails to satisfy the condition that $\cos \psi \leq 0$. The integral curves shown on figure 2(b) reveal that there is one and only one integral curve that can be joined to the curve which represents the front portion of the boundary, and that extends to infinity in the rearward direction with $\cos \psi \leq 0$ at all points. It is the integral curve shown in part (b) that passes through S_U.

A plot of the resulting form for the trace of the cavity boundary is shown in figure 3 for the case in which $\alpha = 1$ and $\mu = 1$. Also indicated on this plot, by dashed lines, are the corresponding results defined by equations (16) and (17) for the case in which there is no ring current.

If $\lambda \neq 0$, the symmetry about the equatorial plane disappears and it is necessary to determine integral curves for the lower half plane as well as the upper. A representative set of integral curves for $\lambda = 11.5^\circ$ is shown in figure 4 for the case $\alpha = 1$, $\mu = 1$. Solutions for small λ are determined in a manner similar to that just described for $\lambda = 0$ by selecting the exterior portions of the integral curves that pass through the singular points. It is thus necessary to consider the lower singular point S_L which is situated at the same geocentric distance as S_U but in the opposite direction from the origin as indicated in figure 4. The resulting curve for the trace of the boundary of the geomagnetic field in the meridian plane containing the sun-earth line is shown in figure 5 for the case $\alpha = 1$, $\mu = 1$. This curve represents the only solution of equation (15) for these values for α and μ that is continuous and satisfies the condition $\cos \psi \leq 0$ at all points. As in figure 3, the dashed line indicates the results from references 1, 2, and 3 for the case in which there is no ring current. It is of interest to observe that the angular coordinates of the neutral points, at which the upper and lower curves join the curve from the forward portion of the boundary, change at a slower rate than the angle between the stream direction and the dipole axis.

As λ is increased it reaches a critical value λ_{cr}, dependent upon the values for α and μ, at which the upper singular point coincides with the upper

neutral point. If λ is increased beyond λ_{cr} the procedures described above to determine the upper rear portion of the boundary no longer apply because the condition $\cos \psi \leq 0$ is violated on the portion of the boundary immediately upstream of the indicated neutral point. The analogous situation for the case of the dipole alone was encountered in reference 1 when λ exceeded 35.6°. A typical example in which a ring current is present is provided by considering the case $\alpha = 1$, $\mu = 1$, $\lambda = 34.5^{\circ}$. The integral curves for this case are shown in figure 6. The dashed line on figure 6 marks the locus of the points at which the integral curves are parallel to the stream, that is, where $\cos \psi = 0$. For the case of the dipole alone this would occur along a straight line, $\theta = \theta_{S_U}$ for $\varphi = +\pi/2$, and $\theta = \theta_{S_L}$ for $\varphi = -\pi/2$. The addition of the ring current alters the situation and the locus is now given by

$$\sin (\theta - \lambda) \left(\frac{2 \cos \theta}{\rho^3} - \bar{B}_{i_\rho} \right) + \cos (\theta - \lambda) \left(\frac{\sin \theta}{\rho^3} - \bar{B}_{i_\theta} \right) = 0 \qquad (19)$$

This equation applies to both families of curves and to both the $\varphi = +\pi/2$ and the $\varphi = -\pi/2$ planes. The only integral curves for which $\cos \psi \neq 0$ at the intersection with this line are the four members of the family shown in figure 6(b) which pass through the singular points S_U and S_L. As in the case of the dipole alone, the desired solution can be obtained by joining the appropriate curves representing the forward and rearward parts of the boundary at the point of intersection with the line given by equation (19). Both portions of the boundary trace are parallel to the direction of the incident stream at this point and satisfy the condition that $\cos \psi \leq 0$ everywhere.

The resulting solution for the trace of the boundary in the meridian plane is shown in figure 7. As in figures 3 and 5, the singular and neutral points are represented by circles and squares and the dashed lines show the corresponding results for the case in which the ring current is absent.

Figures 3, 5, and 7 show the effect of a ring current on the size and shape of the boundary for three different orientations of the dipole axis relative to the stream direction. The principal effect is an over-all enlargement, with some distortion near the front, where the boundary is closest to the ring current.

SOLUTION FOR EQUATORIAL PLANE FOR $\lambda = 0$

For the special case in which $\lambda = 0$, simplification comparable to that in the meridian plane occurs if attention is confined to determining the trace of the boundary in the equatorial plane. Along this plane $\theta = \pi/2$, $\partial\rho/\partial\theta$ vanishes by reason of symmetry, and the governing equation reduces to an ordinary differential equation in which $\partial\rho/\partial\varphi$ can be replaced by $d\rho/d\varphi$. This equation can be solved for $d\rho/d\varphi$, and the result is as follows if attention is restricted to the interval $\pi/2 \leq \varphi \leq 3\pi/2$

$$\frac{d\rho}{d\varphi} = \rho \left[\frac{\rho^6 \sin\varphi \cos\varphi + (1 - b_i\rho^3)\sqrt{\rho^6 - (1 - b_i\rho^3)^2}}{\rho^6 \cos^2\varphi - (1 - b_i\rho^3)^2} \right] \tag{20}$$

where

$$b_i = \frac{2\mu}{\pi\alpha^2}\left(\frac{K}{\alpha + \rho} - \frac{E}{\rho - \alpha}\right) = (\overline{B}_{i_\theta})_{\theta=\pi/2} \tag{21}$$

in which E and K are complete elliptic integrals having the modulus

$$k = \frac{2(\alpha\rho)^{1/2}}{\alpha + \rho} \tag{22}$$

If the intensity of the ring current is zero, μ and, hence, b_i vanish, and equation (20) reduces to the form given in references 1, 2, and 3 for the dipole alone.

The integration constant or starting values to be used in the integration of equation (20) must be such that the curve describing the desired solution intersects the sun-earth line at the same point as the curve describing the trace of the boundary of the hollow in the meridian plane. This signifies that the integral curve of equation (20) that is to be selected to represent the boundary of the hollow must pass through the front singular point of equation (15) with upper signs. That this is the only integral curve of equation (20) which intersects the sun-earth line at a finite distance from the dipole singularity, and hence is an acceptable solution of the original physical problem, is apparent from consideration of the properties of a set of integral curves of equation (20) illustrated in figure 8 for the case defined by $\alpha = 1$ and $\mu = 1$.

Selection of the particular integral curve described in the preceding paragraph yields the curve defining the trace of the cavity boundary in the equatorial plane for the case in which $\lambda = 0$. An isometric view of this curve is illustrated in figure 9, together with the corresponding curve from figure 3 for the trace of the boundary in the meridian plane containing the sun-earth line, for the special case $\alpha = 1$, $\mu = 1$. The corresponding curves for the case of the dipole alone are also indicated in figure 9 by the dashed lines.

RESULTS AND DISCUSSION

The procedures described in the preceding sections enable the calculation of traces of the boundary of the geomagnetic field in the equatorial plane for the case $\lambda = 0$, and in the meridian plane containing the dipole axis and the sun-earth line for various λ, for any given set of values for the velocity and number density of the solar wind and for the strength and radius of the ring

current. The selection of appropriate values to achieve realistic results involves some uncertainties, however, not only because knowledge is meager, but also because the magnitudes of the quantities are believed to vary considerably with time. The results that follow are presented, therefore, for cases involving what are believed to be representative values for these quantities together with results for other cases having smaller and larger values of the governing parameters.

Smith, Coleman, Judge, and Sonett have shown in reference 4 that the magnetometer data from Explorer VI display variations that can be matched closely by results computed assuming the presence of an equatorial ring current of 5 million amperes located at a distance of 60,100 km from the center of the earth and distributed over a cross section having a radius of 3 earth radii or less. This finding forms the basis for the computed forms for the boundary of the cavity that are presented in figures 10 through 13. The results shown in these figures and tabulated in tables I and IIIa are for a ring current of infinitesimal cross section located 60,000 km from the center of the earth.

In the results presented in figure 10, the solar corpuscular stream is assumed to have a number density n in protons/cm^3 and velocity v in cm/sec so that the product nv^2 is equal to 10^{16}. This value would be possessed, for instance, by a stream having a number density of 4 protons/cm^3 and a velocity of 500 km/sec. Such values are representative of conditions observed by Mariner II during quiet times (ref. 20). Results are shown for three different values for the current, namely, 2, 5, and 10 million amperes. The results for no ring current are also indicated by a dashed line. Angles of incidence extending from 0° to 34.5° are included so as to cover the range of angles which the geomagnetic equatorial plane makes with the sun-earth line during the course of the year. The results for $\lambda = 0$ are also shown in isometric projection in figure 11 in order to help visualize the three-dimensional shape of the boundary. The corresponding plots for other λ are not shown because results are available for only the meridian plane. The substantial effects of the ring current in enlarging the size of the cavity are clearly illustrated by the results. It can be seen, for example, that when $\lambda = 0$ the distance to the termination of the geomagnetic field along the sun-earth line increases from about 8.8 to 12.4 earth radii with the addition of a ring current of 5 million amperes to the basic dipole field.

The number density and velocity of the solar wind also have a considerable effect on the dimensions of the cavity. The magnitude of the effect is illustrated in figures 12 and 13 for the case in which the strength of the ring current is 5 million amperes and the product nv^2 takes on several different values between 10^{15} and 10^{17} with n in protons/cm^3 and v in cm/sec. As anticipated, the size of the cavity diminishes rapidly as the intensity of the solar wind increases. Results are not given for nv^2 greater than 10^{17} because part of the boundary approaches so near to the idealized ring current that the simplifying assumption of infinitesimal radius becomes totally inadequate.

Smith, Coleman, Judge, and Sonett have also analyzed the magnetometer data from Pioneer V, which was launched during the recovery phase of a magnetic storm, and have shown in reference 4 that it could be duplicated by results computed

assuming the presence of an equatorial ring current of 5 million amperes located at a distance of 50,000 km from the center of the earth and distributed over a circular cross section having a radius not less than 3 earth radii. These values, which differ from those indicated by the data from Explorer VI only in the distance from the earth to the ring current, form the basis for the selection of the parameters defining the results for the cavity boundary shown in figures 14 through 17 and tabulated in tables II and IIIb. The results are for a ring current of infinitesimal cross section located 50,000 km from the center of the earth. The other parameters are the same as those for which results are shown in figures 10 through 13. Thus, the results presented in figures 14 and 15 illustrate the effect of varying the strength of the ring current, with the number density and velocity of the solar corpuscular stream held fixed at such values that nv^2 is equal to 10^{16}. Those presented in figures 16 and 17 illustrate the effect of varying the intensity of the corpuscular stream with the strength of the ring current maintained fixed at 5 million amperes. It is evident, as is to be expected, that the dimensions of the cavity diminish somewhat as the distance from the earth to the ring current is reduced, other quantities remaining the same. The effect is not overwhelming, however, and the results for the two cases are similar in most qualitative features.

Since the coordinates of the neutral points are of considerable interest, and they cannot be determined accurately from table I or II, a separate listing has been prepared and is presented herein as table IV.

All equations and results presented in the preceding part of this paper are given from the point of view of an observer fixed with respect to the geomagnetic coordinates. It is, however, of equal interest to examine the results from the point of view of an observer fixed with respect to the direction of the solar wind. Figure 18 shows results assembled in this way for the case in which the stream direction is normal to the geographic axis and the geomagnetic axis makes an angle therefrom of $\pm 11.5^{\circ}$, as occurs during the course of the day at the equinoxes, provided the stream direction is assumed parallel to the sun-earth line. Corresponding results for the case in which the geographic equatorial plane is inclined 23° from the stream direction, such as occurs at the solstices, are shown in figure 19. These results show that the boundary of the geomagnetic field is only slightly affected by the diurnal wobbling of the geomagnetic dipole axis relative to the direction of the solar wind. This is particularly true for the dipole alone. The results for this case show that the only part of the boundary that has a marked effect of orientation is that in the immediate vicinity of the neutral points.

Ames Research Center
National Aeronautics and Space Administration
Moffett Field, Calif., Mar. 28, 1963

REFERENCES

1. Spreiter, John R., and Briggs, Benjamin R.: Theoretical Determination of the Form of the Hollow Produced in the Solar Corpuscular Stream by Interaction With the Magnetic Dipole Field of the Earth. NASA TR R-120, 1961.

2. Spreiter, John R., and Briggs, Benjamin R.: Theoretical Determination of the Form of the Boundary of the Solar Corpuscular Stream Produced by Interaction With the Magnetic Dipole Field of the Earth. Jour. Geophys. Res., vol. 67, no. 1, Jan. 1962, pp. 37-51.

3. Spreiter, John R., and Briggs, Benjamin R.: On the Choice of Condition to Apply at the Boundary of the Geomagnetic Field in the Steady-State Chapman-Ferraro Problem. Jour. Geophys. Res., vol. 67, no. 7, July 1962, pp. 2983-2985.

4. Smith, E. J., Coleman, P. J., Judge, D. L., and Sonett, C. P.: Characteristics of the Extraterrestrial Current System: Explorer VI and Pioneer V. Jour. Geophys. Res., vol. 65, no. 6, June 1960, pp. 1858-1861.

5. Kellogg, P. J., and Winckler, J. R.: Cosmic Ray Evidence for a Ring Current. Jour. Geophys. Res., vol. 66, no. 12, Dec. 1961, pp. 3991-4001.

6. Heppner, J. P., Ness, N. F., Scearce, C. S., and Skillman, T. L.: Explorer X Magnetic Field Measurements. Jour. Geophys. Res., vol. 68, no. 1, Jan. 1963, pp. 1-46.

7. Cahill, L. J., and Amazeen, P. G.: The Boundary of the Geomagnetic Field. University of New Hampshire Rep. 62-1, 1962.

8. Spreiter, John R., and Alksne, Alberta Y.: On the Effect of a Ring Current on the Terminal Shape of the Geomagnetic Field. Jour. Geophys. Res., vol. 67, no. 6, June 1962, pp. 2193-2205.

9. Singer, S. F.: A New Model of Magnetic Storms and Aurorae. Transactions, American Geophysical Union, vol. 38, no. 2, Apr. 1957, pp. 175-190.

10. Van Allen, James A., and Frank, Louis A.: Radiation Around the Earth to a Radial Distance of 107,400 km. Nature, vol. 183, no. 4659, Feb. 14, 1959, pp. 430-434.

11. Singer, S. F.: On the Nature and Origin of the Earth's Radiation Belts. Space Research, Hilde Kallmann Bijl, ed., North-Holland Pub. Co., Amsterdam, 1960, pp. 797-820.

12. Chapman, Sydney: Idealized Problems of Plasma Dynamics Relating to Geomagnetic Storms. Reviews of Modern Physics, vol. 32, no. 4, Oct. 1960, pp. 919-933.

13. Dungey, J. W.: Cosmic Electrodynamics. Cambridge University Press, Cambridge, 1958.

14. Stratton, Julius Adams: Electromagnetic Theory. McGraw-Hill Book Co., New York, 1941.

15. Beard, David B.: The Interaction of the Terrestrial Magnetic Field With the Solar Corpuscular Radiation. Jour. Geophys. Res., vol. 65, no. 11, Nov. 1960, pp. 3559-3568.

16. Ferraro, V. C. A.: An Approximate Method of Estimating the Size and Shape of the Stationary Hollow Carved Out in a Neutral Ionized Stream of Corpuscles Impinging on the Geomagnetic Field. Jour. Geophys. Res., vol. 65, no. 12, Dec. 1960, pp. 3951-3953.

17. Davis, Leverett, Jr., and Beard, David B.: A Correction to the Approximate Condition for Locating the Boundary Between a Magnetic Field and a Plasma. Jour. Geophys. Res., vol. 67, no. 11, Oct. 1962, pp. 4505-4507.

18. Hurley, James: Interaction of a Streaming Plasma With the Magnetic Field of a Two-Dimensional Dipole. Physics of Fluids, vol. 4, no. 7, July 1961, pp. 854-859.

19. Slutz, Ralph J.: The Shape of the Geomagnetic Field Boundary Under Uniform External Pressure. Jour. Geophys. Res., vol. 67, no. 2, Feb. 1962, pp. 505-513.

20. Neugebauer, Marcia, and Snyder, Conway W.: The Mission of Mariner II: Preliminary Observations, Solar Plasma Experiment. Science, vol. 138, no. 3545, Dec. 7, 1962, pp. 1095-1097.

TABLE I.- COORDINATES OF THE TRACE OF THE BOUNDARY OF THE GEOMAGNETIC FIELD IN THE MERIDIAN PLANE CONTAINING THE DIPOLE AXIS AND THE SUN-EARTH LINE FOR A RING CURRENT LOCATED AT A GEOCENTRIC DISTANCE OF 60,000 KM

(a) Stream = 10^{16} protons/cm sec^2; ring current = 2 million amperes									(b) Stream = 2.5×10^{16} protons/cm sec^2; ring current = 2 million amperes							
λ deg / θ deg	0	11.5	23.0	34.5	0	11.5	23.0	34.5	0	11.5	23.0	34.5	0	11.5	23.0	34.5
	$\varphi = +\pi/2$				$\varphi = -\pi/2$				$\varphi = +\pi/2$				$\varphi = -\pi/2$			
0	11.55	12.87	14.65	17.26	11.55	12.87	14.65	17.26	9.84	10.96	12.49	14.81	9.84	10.96	12.49	14.81
5	10.86	12.01	13.52	15.72	12.29	13.83	15.94	19.09	9.26	10.23	11.52	13.50	10.47	11.78	13.59	16.37
10	10.23	11.22	12.52	14.39	13.12	14.91	17.44	21.30	8.72	9.56	10.67	12.40	11.17	12.71	14.86	18.26
15	9.65	10.51	11.62	13.26	14.03	16.14	19.19	24.03	8.22	8.95	9.90	11.47	11.95	13.76	16.36	20.59
20	9.29	9.98	10.89	12.35	15.06	17.57	21.30	27.50	7.92	8.59	9.46	10.76	12.83	14.97	18.16	23.55
25	9.31	9.95	10.79	11.90	16.23	19.24	23.88	32.07	7.94	8.57	9.38	10.43	13.83	16.39	20.36	27.47
30	9.34	9.94	10.72	11.73	17.59	21.23	27.13	38.39	7.97	8.56	9.32	10.28	14.98	18.10	23.14	32.88
35	9.38	9.94	10.67	11.59	19.16	23.66	31.36	47.76	8.00	8.57	9.28	10.16	16.33	20.17	26.75	40.91
40	9.43	9.96	10.63	11.47	21.04	26.69	37.14		8.04	8.59	9.25	10.07	17.93	22.76	31.69	
45	9.50	9.99	10.61	11.38	23.31	30.61	45.50		8.10	8.62	9.25	10.00	19.87	26.11	38.83	
50	9.58	10.04	10.62	11.31	26.13	35.87			8.17	8.68	9.27	9.96	22.28	30.61		
55	9.69	10.12	10.65	11.28	29.73	43.35			8.27	8.76	9.32	9.95	25.36	37.00		
60	9.83	10.23	10.70	11.27	34.51				8.41	8.88	9.40	9.98	29.44			
65	10.02	10.38	10.79	11.28	41.18				8.61	9.06	9.53	10.04	35.15			
70	10.26	10.56	10.92	11.33	51.19				8.90	9.30	9.72	10.15	43.70			
75	10.56	10.79	11.07	11.40					9.31	9.64	9.96	10.30				
80	10.87	11.03	11.22	11.46				41.20	9.84	10.04	10.25	10.48				35.18
85	11.12	11.20	11.32	11.47			56.21	34.64	10.31	10.39	10.49	10.61			47.98	29.58
90	11.22	11.23	11.29	11.38			44.39	30.00	10.49	10.50	10.52	10.57			37.89	25.61
95	11.12	11.08	11.07	11.10			36.82	26.54	10.31	10.24	10.19	10.15			31.43	22.65
100	10.87	10.76	10.68	10.65		47.71	31.56	23.85	9.84	9.63	9.41	9.14		40.73	26.93	20.35
105	10.56	10.37	10.22	10.12		39.00	27.68	21.69	9.31	8.97	8.57	8.07		33.29	23.62	18.49
110	10.26	10.01	9.80	9.67	51.19	33.07	24.69	19.90	8.90	8.49	8.07	7.64	43.70	28.22	21.06	16.95
115	10.02	9.72	9.49	9.33	41.18	28.75	22.31	18.40	8.61	8.19	7.80	7.45	35.15	24.52	19.02	15.66
120	9.83	9.51	9.26	9.10	34.51	25.46	20.36	17.11	8.41	7.99	7.63	7.34	29.44	21.71	17.34	14.54
125	9.69	9.34	9.08	8.91	29.73	22.86	18.73	15.98	8.27	7.86	7.51	7.25	25.36	19.48	15.94	13.58
130	9.58	9.21	8.94	8.77	26.13	20.74	17.34	15.00	8.17	7.75	7.42	7.18	22.28	17.67	14.75	12.75
135	9.50	9.11	8.82	8.64	23.31	18.99	16.14	14.13	8.10	7.67	7.34	7.11	19.87	16.17	13.73	12.01
140	9.43	9.02	8.72	8.53	21.04	17.50	15.09	13.36	8.04	7.61	7.28	7.05	17.93	14.90	12.84	11.35
145	9.38	8.95	8.63	8.43	19.16	16.23	14.17	12.66	8.00	7.55	7.22	6.99	16.33	13.82	12.06	10.77
150	9.34	8.88	8.55	8.33	17.59	15.12	13.35	12.03	7.97	7.50	7.16	6.92	14.98	12.87	11.36	10.24
155	9.31	8.83	8.47	8.24	16.23	14.14	12.61	11.46	7.94	7.46	7.10	6.86	13.83	12.04	10.74	9.75
160	9.29	8.77	8.40	8.14	15.06	13.27	11.94	10.93	7.92	7.42	7.05	6.79	12.83	11.31	10.17	9.31
165	9.65	8.97	8.44	8.05	14.03	12.49	11.33	10.44	8.22	7.64	7.19	6.82	11.95	10.64	9.65	8.89
170	10.23	9.46	8.85	8.37	13.12	11.79	10.77	9.98	8.72	8.06	7.55	7.13	11.17	10.04	9.18	8.50
175	10.86	9.98	9.29	8.75	12.29	11.14	10.25	9.55	9.26	8.51	7.92	7.45	10.47	9.49	8.73	8.14
180	11.55	10.54	9.76	9.14	11.55	10.54	9.76	9.14	9.84	8.98	8.31	7.79	9.84	8.98	8.31	7.79
(c) Stream = 10^{15} protons/cm sec^2; ring current = 5 million amperes									(d) Stream = 10^{16} protons/cm sec^2; ring current = 5 million amperes							
0	18.62	20.79	23.73	27.90	18.62	20.79	23.73	27.90	12.25	13.73	15.73	18.74	12.25	13.73	15.73	18.74
5	17.52	19.41	21.91	25.40	19.82	22.35	25.81	30.87	11.53	12.81	14.52	17.08	13.04	14.76	17.12	20.71
10	16.51	18.15	20.30	23.25	21.16	24.10	28.23	34.45	10.87	11.99	13.46	15.68	13.93	15.92	18.73	23.11
15	15.59	17.02	18.86	21.39	22.65	26.10	31.07	38.87	10.26	11.24	12.51	14.50	14.91	17.25	20.63	26.07
20	15.03	16.01	17.57	19.79	24.33	28.41	34.48	44.47	9.99	10.79	11.84	13.56	16.03	18.80	22.92	29.85
25	15.08	15.99	17.21	18.86	26.24	31.12	38.66	51.86	10.04	10.79	11.76	13.03	17.31	20.61	25.72	34.82
30	15.16	15.99	17.10	18.59	28.44	34.35	43.92	62.09	10.11	10.81	11.70	12.86	18.78	22.78	29.25	41.71
35	15.24	16.00	17.02	18.37	31.00	38.28	50.78	77.23	10.20	10.85	11.67	12.73	20.51	25.42	33.85	51.90
40	15.35	16.04	16.96	18.18	34.04	43.19	60.12		10.31	10.91	11.67	12.64	22.56	28.72	40.11	
45	15.46	16.09	16.92	18.02	37.71	49.52	73.65		10.44	11.00	11.70	12.57	25.03	32.97	49.17	
50	15.60	16.15	16.90	17.89	42.27	58.03			10.60	11.12	11.76	12.54	28.10	38.67		
55	15.74	16.23	16.89	17.78	48.09	70.12			10.80	11.27	11.84	12.54	32.01	46.77		
60	15.89	16.31	16.90	17.69	55.81	88.74			11.04	11.45	11.96	12.57	37.19	59.21		
65	16.04	16.40	16.91	17.61	66.60				11.31	11.66	12.09	12.63	44.41			
70	16.19	16.48	16.92	17.53					11.61	11.89	12.25	12.69				
75	16.32	16.55	16.92	17.44					11.91	12.12	12.40	12.76				55.53
80	16.42	16.59	16.89	17.34				66.73	12.17	12.31	12.52	12.80				44.71
85	16.48	16.60	16.84	17.21				56.11	12.35	12.43	12.57	12.78				37.59
90	16.51	16.56	16.74	17.05			71.84	48.60	12.41	12.44	12.52	12.67			48.02	32.55
95	16.48	16.49	16.61	16.85			59.59	43.00	12.35	12.32	12.35	12.44			39.82	28.78
100	16.42	16.37	16.43	16.62		77.17	51.08	38.65	12.17	12.09	12.06	12.10		51.51	34.12	25.85
105	16.32	16.21	16.22	16.35		63.09	44.81	35.16	11.91	11.77	11.68	11.67		42.09	29.90	23.48
110	16.19	16.02	15.98	16.06		53.49	39.98	32.29	11.61	11.40	11.26	11.19		35.67	26.65	21.51
115	16.04	15.82	15.72	15.76	66.60	46.51	36.14	29.87	11.31	11.04	10.84	10.72	44.41	30.98	24.04	19.84
120	15.89	15.61	15.46	15.44	55.81	41.19	32.99	27.79	11.04	10.71	10.47	10.31	37.19	27.40	21.90	18.39
125	15.74	15.40	15.20	15.14	48.09	36.99	30.36	25.98	10.80	10.43	10.15	9.96	32.01	24.57	20.10	17.13
130	15.60	15.20	14.95	14.84	42.27	33.58	28.11	24.38	10.60	10.19	9.88	9.67	28.10	22.26	18.56	16.02
135	15.46	15.02	14.72	14.56	37.71	30.74	26.16	22.95	10.44	9.99	9.66	9.43	25.03	20.33	17.22	15.03
140	15.35	14.84	14.50	14.30	34.04	28.33	24.45	21.67	10.31	9.83	9.47	9.22	22.56	18.70	16.06	14.16
145	15.24	14.69	14.30	14.05	31.00	26.25	22.93	20.51	10.20	9.69	9.31	9.05	20.51	17.29	15.03	13.37
150	15.16	14.54	14.11	13.82	28.44	24.44	21.58	19.45	10.11	9.58	9.17	8.89	18.78	16.07	14.13	12.67
155	15.08	14.41	13.93	13.61	26.24	22.84	20.35	18.48	10.04	9.48	9.05	8.75	17.31	15.00	13.31	12.04
160	15.03	14.29	13.77	13.41	24.33	21.41	19.25	17.59	9.99	9.39	8.94	8.62	16.03	14.05	12.58	11.46
165	15.59	14.46	13.61	13.21	22.65	20.13	18.24	16.77	10.26	9.49	8.88	8.50	14.91	13.21	11.92	10.93
170	16.51	15.23	14.22	13.42	21.16	18.98	17.31	16.01	10.87	10.00	9.31	8.76	13.93	12.45	11.32	10.44
175	17.52	16.06	14.92	14.01	19.82	17.92	16.45	15.30	11.53	10.54	9.76	9.15	13.04	11.75	10.76	9.98
180	18.62	16.95	15.66	14.64	18.62	16.95	15.66	14.64	12.25	11.12	10.24	9.55	12.25	11.12	10.24	9.55

TABLE I.- COORDINATES OF THE TRACE OF THE BOUNDARY OF THE GEOMAGNETIC FIELD IN THE MERIDIAN PLANE CONTAINING THE DIPOLE AXIS AND THE SUN-EARTH LINE FOR A RING CURRENT LOCATED AT A GEOCENTRIC DISTANCE OF 60,000 KM - Concluded

(e) Stream = 2.5×10^{16} protons/cm sec^2; ring current = 5 million amperes									(f) Stream = 10^{17} protons/cm sec^2; ring current = 5 million amperes							
θ deg \ λ deg	0	11.5	23.0	34.5	0	11.5	23.0	34.5	0	11.5	23.0	34.5	0	11.5	23.0	34.5
	$\varphi = +\pi/2$				$\varphi = -\pi/2$				$\varphi = +\pi/2$				$\varphi = -\pi/2$			
0	10.34	11.60	13.30	16.01	10.34	11.60	13.30	16.01	8.00	8.97	10.33	12.74	8.00	8.97	10.33	12.74
5	9.73	10.82	12.27	14.61	11.01	12.46	14.47	17.68	7.53	8.37	9.55	11.68	8.52	9.64	11.24	14.03
10	9.17	10.12	11.37	13.45	11.75	13.45	15.84	19.71	7.10	7.82	8.89	10.82	9.09	10.40	12.30	15.61
15	8.65	9.48	10.56	12.48	12.59	14.58	17.45	22.24	6.69	7.32	8.39	10.13	9.74	11.28	13.55	17.59
20	8.47	9.22	10.21	11.75	13.53	15.89	19.40	25.45	6.58	7.31	8.26	9.63	10.46	12.29	15.06	20.12
25	8.51	9.23	10.15	11.34	14.61	17.43	21.78	29.70	6.61	7.31	8.21	9.36	11.29	13.48	16.91	23.46
30	8.57	9.25	10.11	11.20	15.86	19.27	24.78	35.58	6.65	7.33	8.18	9.24	12.25	14.91	19.26	28.10
35	8.65	9.29	10.09	11.09	17.33	21.52	28.69	44.28	6.70	7.37	8.18	9.16	13.39	16.66	22.31	34.98
40	8.74	9.36	10.10	11.02	19.07	24.33	34.02		6.78	7.43	8.20	9.12	14.74	18.86	26.47	
45	8.87	9.45	10.15	10.99	21.18	27.94	41.72		6.87	7.51	8.26	9.11	16.39	21.68	32.49	
50	9.03	9.58	10.22	10.99	23.80	32.79			7.00	7.63	8.34	9.14	18.44	25.47		
55	9.23	9.74	10.33	11.02	27.13	39.67			7.17	7.80	8.48	9.21	21.05	30.84		
60	9.49	9.96	10.49	11.09	31.53	50.25			7.40	8.03	8.67	9.33	24.50			
65	9.82	10.22	10.68	11.20	37.67				7.74	8.34	8.92	9.51	29.29			
70	10.21	10.54	10.91	11.34					8.23	8.76	9.25	9.74	36.46			
75	10.64	10.88	11.15	11.49				47.18	8.90	9.29	9.66	10.02				36.72
80	11.04	11.18	11.37	11.61				37.99	9.66	9.87	10.09	10.32				29.57
85	11.32	11.39	11.51	11.66				31.94	10.25	10.33	10.42	10.54				24.86
90	11.42	11.44	11.49	11.58			40.77	27.65	10.46	10.47	10.49	10.53			31.72	21.51
95	11.32	11.28	11.28	11.31			33.81	24.44	10.25	10.19	10.14	10.12			26.30	19.00
100	11.04	10.93	10.86	10.83		43.72	28.95	21.93	9.66	9.44	9.19	8.85		34.01	22.51	17.01
105	10.64	10.44	10.29	10.17		35.72	25.36	19.90	8.90	8.43	7.77	6.60		27.78	19.69	15.38
110	10.21	9.93	9.68	9.48		30.25	22.58	18.20	8.23	7.62	6.89	6.02	36.46	23.50	17.50	14.01
115	9.82	9.46	9.15	8.89	37.67	26.26	20.35	16.75	7.74	7.11	6.46	5.82	29.29	20.38	15.73	12.83
120	9.49	9.09	8.74	8.46	31.53	23.21	18.51	15.49	7.40	6.79	6.22	5.70	24.50	17.98	14.26	11.83
125	9.23	8.80	8.43	8.15	27.13	20.79	16.96	14.40	7.17	6.58	6.06	5.63	21.05	16.07	13.04	10.99
130	9.03	8.57	8.20	7.91	23.80	18.81	15.64	13.45	7.00	6.43	5.95	5.57	18.44	14.52	12.01	10.27
135	8.87	8.39	8.01	7.73	21.18	17.16	14.50	12.61	6.87	6.32	5.87	5.52	16.39	13.24	11.14	9.65
140	8.74	8.25	7.86	7.58	19.07	15.77	13.51	11.88	6.78	6.23	5.80	5.47	14.74	12.16	10.39	9.11
145	8.65	8.13	7.74	7.45	17.33	14.58	12.65	11.22	6.70	6.16	5.74	5.42	13.39	11.24	9.74	8.63
150	8.57	8.04	7.63	7.34	15.86	13.55	11.89	10.64	6.65	6.11	5.69	5.38	12.25	10.46	9.17	8.21
155	8.51	7.96	7.54	7.24	14.61	12.65	11.21	10.12	6.61	6.06	5.64	5.33	11.29	9.77	8.66	7.82
160	8.47	7.89	7.45	7.14	13.53	11.85	10.60	9.64	6.58	6.01	5.59	5.29	10.46	9.16	8.20	7.46
165	8.65	8.00	7.49	7.08	12.59	11.14	10.05	9.20	6.69	6.20	5.80	5.49	9.74	8.62	7.78	7.13
170	9.17	8.43	7.85	7.39	11.75	10.50	9.54	8.79	7.10	6.53	6.09	5.74	9.09	8.13	7.39	6.82
175	9.73	8.89	8.24	7.71	11.01	9.92	9.07	8.41	7.53	6.89	6.39	5.99	8.52	7.68	7.03	6.53
180	10.34	9.38	8.64	8.05	10.34	9.38	8.64	8.05	8.00	7.27	6.70	6.25	8.00	7.27	6.70	6.25
(g) Stream = 10^{16} protons/cm sec^2; ring current = 10 million amperes									(h) Stream = 2.5×10^{16} protons/cm sec^2; ring current = 10 million amperes							
0	13.40	15.11	17.42	20.90	13.40	15.11	17.42	20.90	11.19	12.65	14.63	17.80	11.19	12.65	14.63	17.80
5	12.62	14.11	16.09	19.07	14.28	16.25	18.95	23.10	10.54	11.81	13.51	16.26	11.92	13.60	15.92	19.65
10	11.91	13.21	14.92	17.52	15.25	17.54	20.74	25.77	9.94	11.06	12.54	14.99	12.74	14.69	17.44	21.91
15	11.26	12.41	13.89	16.23	16.36	19.02	22.86	29.08	9.40	10.38	11.69	13.94	13.66	15.94	19.23	24.72
20	11.07	11.98	13.17	15.20	17.61	20.75	25.41	33.29	9.33	10.19	11.30	13.12	14.71	17.39	21.39	28.30
25	11.16	12.00	13.09	14.55	19.04	22.77	28.54	38.85	9.41	10.21	11.25	12.61	15.92	19.11	24.04	33.04
30	11.27	12.05	13.06	14.36	20.70	25.20	32.48	46.54	9.51	10.27	11.22	12.44	17.32	21.17	27.38	39.59
35	11.40	12.13	13.05	14.23	22.63	28.15	37.60	57.93	9.64	10.35	11.24	12.35	18.97	23.67	31.73	49.29
40	11.57	12.23	13.08	14.15	24.93	31.83	44.58		9.80	10.46	11.28	12.29	20.92	26.79	37.64	
45	11.76	12.37	13.13	14.10	27.70	36.56	54.67		9.99	10.61	11.36	12.28	23.28	30.81	46.19	
50	11.98	12.53	13.22	14.08	31.12	42.91			10.23	10.80	11.48	12.30	26.19	36.19		
55	12.24	12.72	13.33	14.10	35.48	51.91			10.51	11.02	11.63	12.36	29.89	43.81		
60	12.52	12.93	13.46	14.13	41.24	65.74			10.84	11.29	11.81	12.44	34.78	55.51		
65	12.81	13.16	13.61	14.18	49.26				11.20	11.57	12.01	12.55	41.57			
70	13.10	13.38	13.75	14.24					11.58	11.87	12.23	12.67				
75	13.36	13.57	13.87	14.27				61.95	11.94	12.15	12.43	12.78				
80	13.58	13.72	13.95	14.28				49.88	12.24	12.38	12.58	12.85				42.24
85	13.72	13.81	13.97	14.22				41.94	12.44	12.52	12.65	12.85				35.52
90	13.76	13.80	13.91	14.10			53.41	36.31	12.51	12.53	12.61	12.75			45.16	30.75
95	13.72	13.70	13.75	13.89			44.29	32.10	12.44	12.41	12.44	12.52			37.44	27.17
100	13.58	13.51	13.51	13.59		57.19	37.94	28.82	12.24	12.16	12.13	12.16			32.06	24.37
105	13.36	13.23	13.18	13.22		46.73	33.24	26.16	11.94	11.79	11.70	11.67		39.46	28.07	22.09
110	13.10	12.91	12.80	12.78		39.58	29.61	23.96	11.58	11.36	11.20	11.11		33.40	24.97	20.18
115	12.81	12.56	12.39	12.32	49.26	34.37	26.70	22.07	11.20	10.91	10.68	10.53	41.57	28.98	22.48	18.54
120	12.52	12.20	11.98	11.86	41.24	30.38	24.29	20.44	10.84	10.48	10.19	9.98	34.78	25.58	20.41	17.11
125	12.24	11.86	11.59	11.42	35.48	27.21	22.26	18.99	10.51	10.09	9.76	9.50	29.89	22.88	18.66	15.84
130	11.98	11.56	11.24	11.03	31.12	24.62	20.52	17.71	10.23	9.76	9.39	9.10	26.19	20.66	17.15	14.72
135	11.76	11.28	10.92	10.68	27.70	22.46	19.00	16.57	9.99	9.49	9.08	8.78	23.28	18.81	15.84	13.73
140	11.57	11.04	10.65	10.37	24.93	20.61	17.67	15.55	9.80	9.26	8.83	8.51	20.92	17.23	14.70	12.86
145	11.40	10.84	10.41	10.10	22.63	19.02	16.49	14.63	9.64	9.07	8.62	8.29	18.97	15.88	13.70	12.09
150	11.27	10.66	10.20	9.87	20.70	17.64	15.45	13.81	9.51	8.91	8.44	8.10	17.32	14.71	12.83	11.42
155	11.16	10.51	10.02	9.66	19.04	16.43	14.52	13.07	9.41	8.78	8.29	7.93	15.92	13.69	12.05	10.81
160	11.07	10.38	9.86	9.48	17.61	15.36	13.69	12.41	9.33	8.66	8.16	7.79	14.71	12.80	11.37	10.27
165	11.26	10.36	9.72	9.32	16.36	14.41	12.94	11.81	9.40	8.63	8.05	7.66	13.66	12.00	10.75	9.78
170	11.91	10.89	10.09	9.45	15.25	13.56	12.26	11.26	9.94	9.08	8.39	7.85	12.74	11.30	10.19	9.33
175	12.62	11.47	10.57	9.85	14.28	12.79	11.65	10.75	10.54	9.56	8.79	8.18	11.92	10.66	9.69	8.92
180	13.40	12.10	11.09	10.29	13.40	12.10	11.09	10.29	11.19	10.09	9.22	8.54	11.19	10.09	9.22	8.54

TABLE II.- COORDINATES OF THE TRACE OF THE BOUNDARY OF THE GEOMAGNETIC FIELD IN THE MERIDIAN PLANE CONTAINING THE DIPOLE AXIS AND THE SUN-EARTH LINE FOR A RING CURRENT LOCATED AT A GEOCENTRIC DISTANCE OF 50,000 KM

(a) Stream = 10^{16} protons/cm sec^2; ring current = 2 million amperes

θ deg \ λ deg	0	11.5	23.0	34.5	0	11.5	23.0	34.5
	$\varphi = +\pi/2$				$\varphi = -\pi/2$			
0	11.48	12.77	14.51	16.99	11.48	12.77	14.51	16.99
5	10.80	11.91	13.39	15.46	12.22	13.72	15.79	18.80
10	10.17	11.13	12.40	14.14	13.03	14.79	17.26	20.98
15	9.58	10.42	11.51	12.99	13.94	16.01	18.99	23.67
20	9.18	9.78	10.70	11.99	14.96	17.41	21.07	27.08
25	9.20	9.75	10.49	11.48	16.11	19.06	23.61	31.57
30	9.22	9.73	10.40	11.30	17.44	21.02	26.81	37.78
35	9.25	9.72	10.34	11.15	19.00	23.41	30.98	46.99
40	9.28	9.71	10.28	11.02	20.84	26.40	36.67	
45	9.32	9.72	10.24	10.91	23.07	30.25	44.91	
50	9.38	9.74	10.21	10.82	25.84	35.44		
55	9.44	9.77	10.20	10.74	29.39	42.81		
60	9.52	9.81	10.20	10.68	34.09			
65	9.62	9.88	10.21	10.64	40.68			
70	9.74	9.96	10.24	10.61	50.55			
75	9.88	10.04	10.28	10.58				
80	10.01	10.13	10.30	10.55				40.60
85	10.11	10.18	10.30	10.50			55.45	34.14
90	10.15	10.17	10.25	10.40			43.79	29.57
95	10.11	10.09	10.13	10.23			36.33	26.17
100	10.01	9.95	9.95	10.01		47.10	31.15	23.53
105	9.88	9.77	9.73	9.77		38.51	27.33	21.41
110	9.74	9.60	9.53	9.54	50.55	32.66	24.39	19.67
115	9.62	9.45	9.34	9.33	40.68	28.41	22.06	18.21
120	9.52	9.32	9.19	9.15	34.09	25.17	20.15	16.95
125	9.44	9.21	9.06	9.00	29.39	22.62	18.56	15.87
130	9.38	9.11	8.94	8.86	25.84	20.55	17.20	14.91
135	9.32	9.03	8.84	8.74	23.07	18.82	16.03	14.07
140	9.28	8.96	8.75	8.63	20.84	17.37	15.01	13.31
145	9.25	8.90	8.66	8.52	19.00	16.12	14.10	12.62
150	9.22	8.85	8.58	8.42	17.44	15.02	13.29	12.00
155	9.20	8.79	8.51	8.32	16.11	14.06	12.56	11.43
160	9.18	8.75	8.43	8.23	14.96	13.20	11.90	10.91
165	9.58	8.92	8.40	8.13	13.94	12.43	11.29	10.42
170	10.17	9.42	8.82	8.35	13.03	11.73	10.73	9.96
175	10.80	9.94	9.26	8.72	12.22	11.08	10.21	9.53
180	11.48	10.49	9.72	9.12	11.48	10.49	9.72	9.12

(b) Stream = 2.5×10^{16} protons/cm sec^2; ring current = 2 million amperes

θ deg \ λ deg	0	11.5	23.0	34.5	0	11.5	23.0	34.5
	$\varphi = +\pi/2$				$\varphi = -\pi/2$			
0	9.80	10.91	12.40	14.55	9.80	10.91	12.40	14.55
5	9.22	10.17	11.44	13.24	10.43	11.72	13.49	16.10
10	8.68	9.51	10.59	12.12	11.13	12.63	14.75	17.96
15	8.18	8.90	9.83	11.15	11.90	13.67	16.23	20.26
20	7.85	8.40	9.14	10.34	12.77	14.88	18.01	23.18
25	7.87	8.38	9.06	9.95	13.76	16.28	20.18	27.03
30	7.88	8.36	8.99	9.80	14.90	17.96	22.92	32.35
35	7.91	8.36	8.93	9.67	16.23	20.01	26.49	40.24
40	7.94	8.36	8.89	9.57	17.81	22.57	31.36	
45	7.98	8.37	8.86	9.48	19.72	25.87	38.42	
50	8.03	8.40	8.85	9.41	22.09	30.30		
55	8.10	8.44	8.86	9.36	25.13	36.62		
60	8.19	8.50	8.88	9.33	29.16			
65	8.31	8.59	8.93	9.33	34.79			
70	8.47	8.72	9.00	9.34	43.24			
75	8.68	8.87	9.10	9.37				
80	8.92	9.05	9.21	9.41				34.74
85	9.12	9.19	9.28	9.41			47.43	29.21
90	9.20	9.22	9.26	9.33			37.46	25.30
95	9.12	9.08	9.07	9.09			31.08	22.39
100	8.92	8.82	8.75	8.71		40.29	26.64	20.12
105	8.68	8.52	8.39	8.31		32.94	23.37	18.31
110	8.47	8.27	8.11	8.01	43.24	27.93	20.86	16.81
115	8.31	8.08	7.90	7.80	34.79	24.29	18.85	15.55
120	8.19	7.94	7.75	7.65	29.16	21.52	17.22	14.47
125	8.10	7.83	7.64	7.53	25.13	19.33	15.85	13.54
130	8.03	7.75	7.54	7.43	22.09	17.55	14.69	12.72
135	7.98	7.68	7.46	7.34	19.72	16.08	13.68	12.00
140	7.94	7.62	7.39	7.26	17.81	14.83	12.81	11.35
145	7.91	7.57	7.33	7.18	16.23	13.76	12.03	10.77
150	7.88	7.52	7.26	7.10	14.90	12.83	11.34	10.24
155	7.87	7.48	7.20	7.03	13.76	12.00	10.72	9.75
160	7.85	7.44	7.14	6.95	12.77	11.27	10.16	9.31
165	8.18	7.62	7.17	6.87	11.90	10.61	9.64	8.89
170	8.68	8.04	7.53	7.13	11.13	10.01	9.16	8.50
175	9.22	8.48	7.91	7.45	10.43	9.46	8.72	8.13
180	9.80	8.96	8.30	7.78	9.80	8.96	8.30	7.78

(c) Stream = 10^{15} protons/cm sec^2; ring current = 5 million amperes

θ deg \ λ deg	0	11.5	23.0	34.5	0	11.5	23.0	34.5
	$\varphi = +\pi/2$				$\varphi = -\pi/2$			
0	18.10	20.16	22.94	26.86	18.10	20.16	22.94	26.86
5	17.03	18.81	21.17	24.44	19.27	21.66	24.95	29.73
10	16.04	17.59	19.61	22.35	20.56	23.35	27.28	33.17
15	15.13	16.47	18.21	20.53	21.99	25.28	30.02	37.42
20	14.51	15.45	16.94	18.94	23.61	27.50	33.30	42.81
25	14.55	15.37	16.48	18.00	25.44	30.11	37.32	49.90
30	14.59	15.34	16.35	17.73	27.55	33.21	42.37	59.73
35	14.65	15.33	16.25	17.49	30.01	36.99	48.97	74.28
40	14.71	15.33	16.16	17.28	32.92	41.71	57.95	
45	14.78	15.33	16.09	17.10	36.45	47.80	70.99	
50	14.86	15.35	16.03	16.95	40.83	55.99		
55	14.94	15.37	15.98	16.81	46.42	67.64		
60	15.03	15.40	15.94	16.68	53.86			
65	15.11	15.43	15.90	16.56	64.25			
70	15.19	15.46	15.86	16.44				
75	15.26	15.47	15.82	16.33				
80	15.31	15.47	15.76	16.20				64.19
85	15.35	15.46	15.69	16.07			87.63	53.98
90	15.36	15.42	15.60	15.92			69.21	46.76
95	15.35	15.36	15.49	15.75			57.42	41.38
100	15.31	15.28	15.36	15.57		74.41	49.22	37.20
105	15.26	15.17	15.21	15.37		60.84	43.19	33.86
110	15.19	15.05	15.04	15.15		51.60	38.56	31.11
115	15.11	14.92	14.86	14.93	64.25	44.88	34.87	28.81
120	15.03	14.79	14.68	14.70	53.86	39.77	31.86	26.83
125	14.94	14.65	14.50	14.48	46.42	35.74	29.34	25.12
130	14.86	14.52	14.33	14.26	40.83	32.47	27.20	23.61
135	14.78	14.39	14.15	14.04	36.45	29.75	25.34	22.26
140	14.71	14.27	13.99	13.84	32.92	27.44	23.72	21.05
145	14.65	14.16	13.83	13.64	30.01	25.46	22.28	19.95
150	14.59	14.05	13.68	13.45	27.55	23.72	20.99	18.95
155	14.55	13.95	13.53	13.26	25.44	22.19	19.82	18.04
160	14.51	13.86	13.39	13.08	23.61	20.83	18.76	17.19
165	15.13	14.07	13.26	12.91	21.99	19.60	17.79	16.40
170	16.04	14.84	13.88	13.13	20.56	18.48	16.90	15.67
175	17.03	15.65	14.57	13.71	19.27	17.46	16.07	14.98
180	18.10	16.52	15.29	14.33	18.10	16.52	15.29	14.33

(d) Stream = 10^{16} protons/cm sec^2; ring current = 5 million amperes

θ deg \ λ deg	0	11.5	23.0	34.5	0	11.5	23.0	34.5
	$\varphi = +\pi/2$				$\varphi = -\pi/2$			
0	12.06	13.46	15.37	18.11	12.06	13.46	15.37	18.11
5	11.34	12.56	14.18	16.48	12.84	14.47	16.72	20.03
10	10.69	11.75	13.14	15.09	13.70	15.61	18.28	22.35
15	10.09	11.01	12.21	13.90	14.66	16.90	20.13	25.22
20	9.74	10.42	11.36	12.90	15.75	18.40	22.34	28.86
25	9.77	10.40	11.24	12.36	16.99	20.16	25.05	33.66
30	9.82	10.40	11.17	12.18	18.41	22.25	28.47	40.30
35	9.88	10.42	11.12	12.04	20.08	24.80	32.92	50.14
40	9.95	10.44	11.09	11.92	22.05	27.99	38.98	
45	10.04	10.49	11.07	11.83	24.44	32.10	47.76	
50	10.14	10.55	11.08	11.76	27.40	37.63		
55	10.26	10.63	11.10	11.71	31.18	45.48		
60	10.40	10.72	11.14	11.68	36.19	57.55		
65	10.56	10.83	11.20	11.67	43.19			
70	10.73	10.95	11.25	11.66	53.69			
75	10.89	11.06	11.31	11.65				
80	11.03	11.15	11.34	11.62				43.29
85	11.12	11.20	11.34	11.56				36.41
90	11.16	11.19	11.28	11.45			46.60	31.53
95	11.12	11.11	11.16	11.29			38.65	27.89
100	11.03	10.97	10.98	11.07		50.05	33.13	25.07
105	10.89	10.79	10.76	10.80		40.92	29.06	22.79
110	10.73	10.58	10.51	10.51	53.69	34.69	25.92	20.92
115	10.56	10.37	10.26	10.23	43.19	30.15	23.42	19.34
120	10.40	10.17	10.02	9.96	36.19	26.70	21.37	17.98
125	10.26	9.99	9.81	9.72	31.18	23.97	19.65	16.79
130	10.14	9.83	9.62	9.51	27.40	21.75	18.19	15.75
135	10.04	9.70	9.46	9.32	24.44	19.90	16.92	14.82
140	9.95	9.58	9.31	9.15	22.05	18.33	15.81	13.99
145	9.88	9.47	9.18	9.00	20.08	16.99	14.82	13.24
150	9.82	9.38	9.07	8.86	18.41	15.81	13.95	12.56
155	9.77	9.30	8.96	8.73	16.99	14.78	13.16	11.94
160	9.74	9.23	8.86	8.61	15.75	13.86	12.45	11.38
165	10.09	9.36	8.78	8.49	14.66	13.03	11.80	10.85
170	10.69	9.86	9.21	8.69	13.70	12.29	11.21	10.37
175	11.34	10.40	9.66	9.08	12.84	11.61	10.66	9.91
180	12.06	10.98	10.14	9.48	12.06	10.98	10.14	9.48

TABLE II.- COORDINATES OF THE TRACE OF THE BOUNDARY OF THE GEOMAGNETIC FIELD IN THE MERIDIAN PLANE CONTAINING THE DIPOLE AXIS AND THE SUN-EARTH LINE FOR A RING CURRENT LOCATED AT A GEOCENTRIC DISTANCE OF 50,000 KM - Concluded

(e) Stream = 2.5×10^{16} protons/cm sec^2; ring current = 5 million amperes									(f) Stream = 10^{17} protons/cm sec^2; ring current = 5 million amperes							
λ deg / θ deg	0	11.5	23.0	34.5	0	11.5	23.0	34.5	0	11.5	23.0	34.5	0	11.5	23.0	34.5
	$\varphi = +\pi$ 2				$\varphi = -\pi$ 2				$\varphi = +\pi$ 2				$\varphi = -\pi$ 2			
0	10.23	11.43	13.06	15.47	10.23	11.43	13.06	15.47	7.97	8.91	10.19	12.23	7.97	8.91	10.19	12.23
5	9.63	10.67	12.06	14.09	10.89	12.29	14.21	17.10	7.50	8.31	9.40	11.17	8.49	9.58	11.09	13.51
10	9.07	9.98	11.17	12.92	11.63	13.26	15.55	19.08	7.07	7.77	8.70	10.28	9.06	10.33	12.13	15.06
15	8.56	9.35	10.37	11.92	12.45	14.36	17.12	21.53	6.66	7.28	8.08	9.54	9.69	11.19	13.36	16.98
20	8.29	8.92	9.75	11.12	13.37	15.63	19.01	24.64	6.48	7.07	7.84	9.00	10.41	12.19	14.84	19.43
25	8.32	8.91	9.68	10.69	14.42	17.13	21.32	28.74	6.50	7.07	7.79	8.72	11.23	13.36	16.65	22.67
30	8.36	8.91	9.62	10.55	15.64	18.92	24.24	34.42	6.54	7.07	7.75	8.60	12.18	14.77	18.94	27.14
35	8.42	8.93	9.59	10.43	17.06	21.10	28.03	42.83	6.58	7.09	7.73	8.51	13.29	16.48	21.92	33.78
40	8.49	8.97	9.57	10.34	18.74	23.82	33.21		6.64	7.13	7.73	8.45	14.62	18.61	25.98	44.67
45	8.57	9.02	9.58	10.27	20.79	27.33	40.70		6.71	7.18	7.75	8.41	16.22	21.37	31.86	
50	8.68	9.09	9.60	10.23	23.31	32.05			6.81	7.26	7.79	8.41	18.21	25.07		
55	8.81	9.19	9.65	10.22	26.54	38.74			6.94	7.37	7.87	8.43	20.75	30.33		
60	8.98	9.31	9.72	10.22	30.82				7.11	7.53	7.98	8.48	24.12			
65	9.18	9.46	9.82	10.25	36.80				7.35	7.73	8.14	8.57	28.80			
70	9.40	9.64	9.93	10.29	45.75				7.67	8.00	8.34	8.70	35.82			
75	9.64	9.82	10.05	10.34					8.08	8.32	8.58	8.86				
80	9.86	9.98	10.14	10.37				36.93	8.52	8.66	8.82	9.01				28.95
85	10.01	10.08	10.19	10.35				31.05	8.85	8.92	9.00	9.11				24.34
90	10.07	10.09	10.15	10.26			39.72	26.89	8.98	8.99	9.02	9.07			31.12	21.07
95	10.01	9.99	10.01	10.07			32.95	23.78	8.85	8.81	8.79	8.78			25.81	18.63
100	9.86	9.78	9.76	9.78		42.65	28.23	21.36	8.52	8.39	8.27	8.17		33.41	22.11	16.72
105	9.64	9.51	9.44	9.42		34.86	24.76	19.42	8.08	7.84	7.59	7.32		27.30	19.37	15.17
110	9.40	9.22	9.10	9.03	45.75	29.55	22.07	17.80	7.67	7.34	7.01	6.67	35.82	23.12	17.25	13.88
115	9.18	8.95	8.78	8.69	36.80	25.68	19.93	16.44	7.35	6.98	6.63	6.31	28.80	20.08	15.56	12.79
120	8.98	8.71	8.52	8.39	30.82	22.73	18.17	15.27	7.11	6.73	6.39	6.10	24.12	17.75	14.16	11.84
125	8.81	8.52	8.30	8.15	26.54	20.39	16.69	14.24	6.94	6.55	6.22	5.96	20.75	15.91	12.99	11.03
130	8.68	8.36	8.12	7.96	23.31	18.49	15.44	13.34	6.81	6.42	6.10	5.86	18.21	14.41	11.99	10.32
135	8.57	8.22	7.97	7.80	20.79	16.91	14.35	12.54	6.71	6.32	6.01	5.77	16.22	13.16	11.14	9.70
140	8.49	8.11	7.84	7.66	18.74	15.57	13.40	11.83	6.64	6.24	5.93	5.70	14.62	12.11	10.40	9.16
145	8.42	8.02	7.73	7.53	17.06	14.41	12.56	11.20	6.58	6.17	5.86	5.63	13.29	11.21	9.75	8.68
150	8.36	7.94	7.63	7.42	15.64	13.41	11.82	10.62	6.54	6.12	5.80	5.57	12.18	10.43	9.18	8.24
155	8.32	7.87	7.55	7.32	14.42	12.53	11.15	10.10	6.50	6.07	5.75	5.51	11.23	9.75	8.66	7.84
160	8.29	7.81	7.46	7.22	13.37	11.75	10.55	9.63	6.48	6.03	5.69	5.46	10.41	9.14	8.20	7.48
165	8.56	7.94	7.44	7.13	12.45	11.05	10.00	9.19	6.66	6.18	5.80	5.49	9.69	8.60	7.78	7.15
170	9.07	8.37	7.81	7.37	11.63	10.42	9.50	8.78	7.07	6.52	6.08	5.74	9.06	8.11	7.39	6.83
175	9.63	8.82	8.19	7.69	10.89	9.84	9.03	8.40	7.50	6.87	6.38	5.99	8.49	7.67	7.03	6.54
180	10.23	9.31	8.60	8.04	10.23	9.31	8.60	8.04	7.97	7.26	6.70	6.26	7.97	7.26	6.70	6.26
(g) Stream = 10^{16} protons/cm sec^2; ring current = 10 million amperes									(h) Stream = 2.5×10^{16} protons/cm sec^2; ring current = 10 million amperes							
0	12.99	14.57	16.70	19.79	12.99	14.57	16.70	19.79	10.95	12.30	14.13	16.86	10.95	12.30	14.13	16.86
5	12.23	13.60	15.42	18.02	13.84	15.66	18.16	21.88	10.30	11.48	13.04	15.38	11.66	13.22	15.37	18.64
10	11.53	12.73	14.29	16.52	14.78	16.90	19.87	24.42	9.72	10.74	12.09	14.12	12.45	14.27	16.82	20.80
15	10.89	11.94	13.29	15.24	15.83	18.31	21.89	27.55	9.18	10.08	11.25	13.06	13.34	15.47	18.53	23.47
20	10.59	11.36	12.40	14.19	17.02	19.95	24.31	31.54	8.97	9.69	10.63	12.21	14.35	16.86	20.59	26.87
25	10.65	11.36	12.30	13.55	18.38	21.87	27.27	36.79	9.03	9.70	10.56	11.71	15.50	18.49	23.12	31.35
30	10.72	11.38	12.24	13.38	19.94	24.16	31.00	44.05	9.10	9.72	10.52	11.56	16.83	20.45	26.29	37.55
35	10.82	11.42	12.21	13.23	21.77	26.96	35.86	54.82	9.20	9.77	10.50	11.45	18.39	22.83	30.43	46.73
40	10.93	11.48	12.19	13.12	23.93	30.44	42.48		9.31	9.84	10.51	11.37	20.24	25.80	36.07	
45	11.06	11.55	12.20	13.04	26.55	34.93	52.07		9.44	9.93	10.54	11.32	22.47	29.62	44.23	
50	11.20	11.65	12.23	12.99	29.78	40.96			9.60	10.04	10.60	11.29	25.23	34.75		
55	11.37	11.76	12.28	12.95	33.91	49.52			9.79	10.18	10.68	11.29	28.75	42.03		
60	11.54	11.88	12.34	12.93	39.38	62.68			10.00	10.34	10.78	11.32	33.41	53.22		
65	11.73	12.01	12.40	12.92	47.01				10.23	10.52	10.89	11.35	39.90			
70	11.91	12.14	12.47	12.91					10.47	10.70	11.00	11.40				
75	12.07	12.25	12.52	12.89				58.77	10.69	10.87	11.11	11.43				50.01
80	12.20	12.33	12.54	12.85				47.32	10.88	11.00	11.18	11.44				40.26
85	12.28	12.37	12.53	12.78				39.79	11.00	11.07	11.20	11.40				33.85
90	12.31	12.35	12.46	12.66			50.82	34.46	11.04	11.07	11.15	11.30			43.19	29.31
95	12.28	12.28	12.34	12.49			42.16	30.48	11.00	10.98	11.02	11.12			35.82	25.92
100	12.20	12.15	12.17	12.28		54.52	36.12	27.38	10.88	10.82	10.81	10.87		46.30	30.69	23.27
105	12.07	11.97	11.95	12.01		44.56	31.67	24.89	10.69	10.58	10.53	10.55		37.83	26.89	21.14
110	11.91	11.76	11.70	11.72		37.77	28.24	22.83	10.47	10.31	10.21	10.19		32.05	23.96	19.36
115	11.73	11.53	11.42	11.41	47.01	32.82	25.50	21.08	10.23	10.02	9.88	9.81	39.90	27.84	21.62	17.86
120	11.54	11.30	11.15	11.09	39.38	29.04	23.25	19.58	10.00	9.74	9.56	9.45	33.41	24.62	19.68	16.55
125	11.37	11.08	10.89	10.79	33.91	26.06	21.36	18.26	9.79	9.48	9.26	9.12	28.75	22.07	18.06	15.40
130	11.20	10.87	10.64	10.51	29.78	23.62	19.74	17.09	9.60	9.26	9.00	8.83	25.23	19.98	16.66	14.39
135	11.06	10.68	10.41	10.25	26.55	21.59	18.33	16.05	9.44	9.06	8.78	8.58	22.47	18.24	15.45	13.48
140	10.93	10.51	10.21	10.02	23.93	19.86	17.10	15.11	9.31	8.89	8.58	8.37	20.24	16.76	14.39	12.68
145	10.82	10.36	10.03	9.81	21.77	18.38	16.00	14.27	9.20	8.75	8.41	8.18	18.39	15.49	13.45	11.96
150	10.72	10.23	9.86	9.62	19.94	17.08	15.03	13.50	9.10	8.63	8.27	8.02	16.83	14.38	12.62	11.31
155	10.65	10.11	9.72	9.44	18.38	15.94	14.16	12.81	9.03	8.52	8.14	7.87	15.50	13.41	11.88	10.73
160	10.59	10.01	9.58	9.28	17.02	14.92	13.37	12.18	8.97	8.43	8.03	7.74	14.35	12.56	11.22	10.20
165	10.89	10.07	9.46	9.14	15.83	14.02	12.65	11.60	9.18	8.47	7.93	7.62	13.34	11.79	10.62	9.72
170	11.53	10.60	9.86	9.28	14.78	13.20	12.00	11.07	9.72	8.92	8.28	7.78	12.45	11.10	10.07	9.27
175	12.23	11.17	10.34	9.68	13.84	12.46	11.40	10.57	10.30	9.40	8.68	8.12	11.66	10.48	9.57	8.86
180	12.99	11.79	10.85	10.11	12.99	11.79	10.85	10.11	10.95	9.92	9.11	8.48	10.95	9.92	9.11	8.48

TABLE III.- COORDINATES OF THE TRACE OF THE BOUNDARY OF THE GEOMAGNETIC FIELD IN THE GEOMAGNETIC EQUATORIAL PLANE; $\lambda = 0^{\circ}$

	(a) Geocentric distance to ring current = 60,000 km								(b) Geocentric distance to ring current = 50,000 km							
nv^2 / λ deg	10^{16}	2.5×10^{16}	10^{15}	10^{16}	2.5×10^{16} ×	10^{17}	10^{16}	2.5×10^{16}	10^{16}	2.5×10^{16}	10^{15}	10^{16}	2.5×10^{16}	10^{17}	10^{16}	2.5×10^{16}
	2 million amps		5 million amps				10 million amps		2 million amps		5 million amps				10 million amps	
90.0	11.22	10.49	16.51	12.41	11.42	10.46	13.76	12.51	10.15	9.20	15.36	11.16	10.07	8.98	12.31	11.04
95.0	11.22	10.49	16.52	12.42	11.43	10.46	13.77	12.51	10.15	9.21	15.37	11.16	10.07	8.98	12.32	11.05
100.0	11.24	10.50	16.55	12.44	11.44	10.47	13.80	12.53	10.17	9.22	15.41	11.19	10.09	8.99	12.34	11.07
105.0	11.27	10.52	16.61	12.48	11.47	10.49	13.84	12.57	10.21	9.25	15.46	11.22	10.12	9.01	12.39	11.10
110.0	11.31	10.55	16.70	12.53	11.51	10.51	13.90	12.62	10.25	9.28	15.55	11.27	10.16	9.04	12.44	11.15
115.0	11.36	10.59	16.81	12.59	11.56	10.54	13.98	12.68	10.31	9.33	15.65	11.34	10.21	9.07	12.52	11.21
120.0	11.43	10.64	16.94	12.68	11.62	10.58	14.08	12.76	10.39	9.38	15.79	11.42	10.28	9 11	12.61	11.29
125.0	11.52	10.70	17.11	12.78	11.70	10.63	14.20	12.86	10.48	9.45	15.95	11.53	10.36	9.17	12.73	11.38
130.0	11.62	10.77	17.30	12.90	11.80	10.69	14.34	12.97	10.59	9.54	16.13	11.65	10.46	9.23	12.87	11.50
135.0	11.74	10.85	17.53	13.04	11.91	10.77	14.50	13.11	10.72	9.64	16.36	11.79	10.57	9.31	13.02	11.63
140.0	11.88	10.96	17.79	13.21	12.04	10.85	14.70	13.27	10.87	9.76	16.61	11.96	10.71	9.40	13.21	11.78
145.0	12.04	11.08	18.10	13.40	12.19	10.95	14.92	13.45	11.05	9.89	16.90	12.15	10.86	9.50	13.42	11.96
150.0	12.23	11.22	18.44	13.62	12.37	11.08	15.17	13.66	11.25	10.05	17.24	12.36	11.04	9.63	13.67	12.16
155.0	12.45	11.39	18.84	13.87	12.58	11.22	15.47	13.91	11.48	10.24	17.62	12.61	11.25	9.78	13.94	12.40
160.0	12.71	11.59	19.28	14.16	12.82	11.39	15.80	14.19	11.74	10.45	18.05	12.90	11.49	9.95	14.26	12.66
165.0	13.00	11.83	19.80	14.50	13.09	11.59	16.19	14.51	12.04	10.70	18.54	13.23	11.76	10.15	14.62	12.97
170.0	13.34	12.10	20.38	14.88	13.41	11.83	16.63	14.88	12.39	10.98	19.10	13.60	12.07	10.38	15.04	13.32
175.0	13.73	12.42	21.04	15.32	13.78	12.11	17.13	15.31	12.78	11.31	19.73	14.03	12.43	10.66	15.51	13.72
180.0	14.19	12.80	21.80	15.83	14.21	12.44	17.71	15.80	13.23	11.69	20.46	14.51	12.85	10.97	16.05	14.19
185.0	14.71	13.24	22.67	16.42	14.71	12.83	18.37	16.37	13.75	12.13	21.29	15.08	13.33	11.35	16.67	14.72
190.0	15.32	13.76	23.67	17.10	15.30	13.29	19.14	17.04	14.36	12.64	22.24	15.73	13.88	11.79	17.39	15.34
195.0	16.03	14.37	24.83	17.90	15.98	13.84	20.04	17.81	15.05	13.24	23.35	16.48	14.53	12.30	18.23	16.06
200.0	16.87	15.09	26.18	18.83	16.79	14.49	21.09	18.72	15.87	13.94	24.63	17.37	15.29	12.91	19.20	16.90
205.0	17.86	15.94	27.77	19.93	17.74	15.27	22.33	19.80	16.82	14.76	26.14	18.41	16.19	13.63	20.35	17.89
210.0	19.04	16.97	29.65	21.24	18.89	16.21	23.80	21.08	17.96	15.75	27.93	19.64	17.26	14.50	21.71	19.07
215.0	20.46	18.21	31.91	22.82	20.27	17.35	25.58	22.63	19.33	16.93	30.08	21.13	18.55	15.55	23.35	20.50
220.0	22.20	19.73	34.67	24.75	21.96	18.75	27.75	24.53	21.00	18.38	32.69	22.94	20.13	16.84	25.35	22.23
225.0	24.36	21.62	38.08	27.15	24.06	20.51	30.44	26.88	23.06	20.17	35.93	25.18	22.08	18.45	27.83	24.39
230.0	27.09	24.02	42.39	30.18	26.73	22.75	33.84	29.87	25.67	22.44	40.01	28.02	24.55	20.49	30.96	27.12
235.0	30.64	27.15	48.00	34.13	30.21	25.67	38.28	33.76	29.06	25.39	45.32	31.71	27.77	23.15	35.04	30.68
240.0	35.43	31.37	55.54	39.46	34.90	29.62	44.25	39.01	33.63	29.36	52.45	36.68	32.11	26.74	40.52	35.47
245.0	42.19	37.34	66.18	46.98	41.53	35.21	52.69	46.43	40.07	34.98	62.51	43.70	38.24	31.81	48.27	42.23
250.0	52.41	46.36	82.24	58.35	51.56	43.68	65.44	57.64	49.79	43.46	77.70	54.29	47.50	39.49	59.97	52.45
255.0	69.54	61.49	109.15	77.41	68.37	57.89	86.81	76.45	66.09	57.66	103.14	72.04	63.01	52.36	79.57	69.58

TABLE IV.- COORDINATES OF THE NEUTRAL POINTS

nv^2, protons per cm sec^2	i, amp	λ, deg	Ring current at 60,000 km				Ring current at 50,000 km			
			θ_{N_U}, deg	ρ_{N_U}, earth radii	θ_{N_L}, deg	ρ_{N_L}, earth radii	θ_{N_U}, deg	ρ_{N_U}, earth radii	θ_{N_L}, deg	ρ_{N_L}, earth radii
10^{16}	2×10^6	0	18.3	9.28	161.7	9.28	18.6	9.18	161.4	9.18
		11.5	19.0	9.98	162.6	8.74	19.9	9.78	162.8	8.72
		23	19.5	10.89	163.8	8.34	20.9	10.56	164.6	8.36
		34.5	23.9	11.95	165.4	8.04	23.5	11.54	166.6	8.10
2.5×10^{16}	2×10^6	0	18.1	7.92	161.9	7.92	18.5	7.85	161.5	7.85
		11.5	18.1	8.59	162.0	7.40	19.4	8.41	162.5	7.42
		23	17.8	9.49	162.6	7.02	20.0	9.14	163.9	7.10
		34.5	23.9	10.47	163.7	6.75	23.5	10.00	165.7	6.86
10^{15}	5×10^6	0	18.3	15.00	161.7	15.00	18.7	14.50	161.3	14.50
		11.5	19.8	16.00	163.4	14.22	20.2	15.40	163.2	13.80
		23	21.0	17.31	165.3	13.60	21.6	16.57	165.2	13.25
		34.5	24.3	18.90	167.4	13.12	23.7	18.08	167.4	12.83
10^{16}	5×10^6	0	17.5	9.97	162.5	9.97	18.2	9.73	161.8	9.73
		11.5	18.2	10.79	163.4	9.33	19.4	10.42	163.2	9.19
		23	18.6	11.93	164.6	8.84	20.3	11.32	164.8	8.77
		34.5	25.2	13.02	166.1	8.47	24.3	12.38	166.7	8.45
2.5×10^{16}	5×10^6	0	17.1	8.45	162.9	8.45	17.9	8.28	162.1	8.28
		11.5	17.2	9.22	163.1	7.84	18.7	8.92	163.1	7.78
		23	17.0	10.26	163.6	7.39	19.2	9.76	164.3	7.40
		34.5	25.4	11.33	164.6	7.06	24.5	10.71	166.0	7.11
10^{17}	5×10^6	0	16.7	6.56	163.3	6.56	17.6	6.47	162.4	6.47
		11.5	15.1	7.31	162.0	6.00	17.2	7.08	162.4	6.01
		23	16.9	8.31	161.0	5.58	16.7	7.89	162.6	5.67
		34.5	25.5	9.34	160.5	5.28	24.7	8.72	163.4	5.41
10^{16}	10×10^6	0	16.9	11.03	163.1	11.03	17.7	10.57	162.3	10.57
		11.5	18.0	11.97	164.3	10.28	19.0	11.36	163.7	9.94
		23	18.8	13.19	165.7	9.70	20.1	12.38	165.4	9.45
		34.5	26.3	14.49	167.4	9.24	25.1	13.55	167.4	9.07
2.5×10^{16}	10×10^6	0	16.1	9.28	163.9	9.28	17.3	8.95	162.7	8.95
		11.5	16.6	10.18	164.4	8.58	18.2	9.68	163.8	8.37
		23	18.2	11.33	165.3	8.04	19.0	10.64	165.2	7.92
		34.5	27.4	12.51	166.5	7.62	25.9	11.68	166.8	7.58

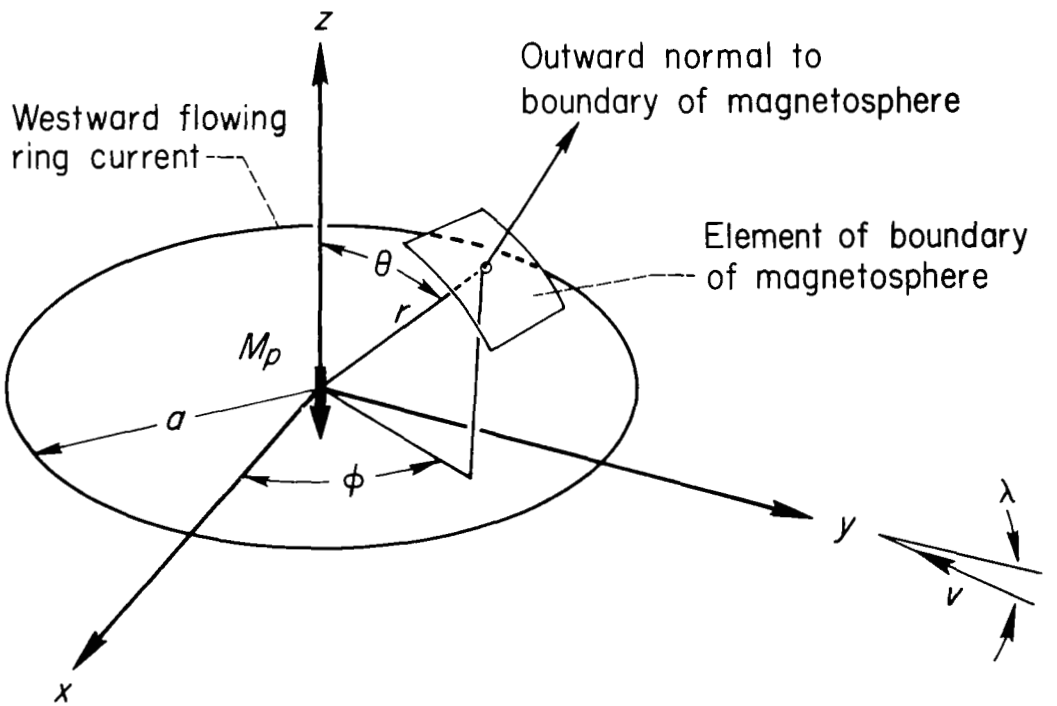

Figure 1.- View of coordinate system.

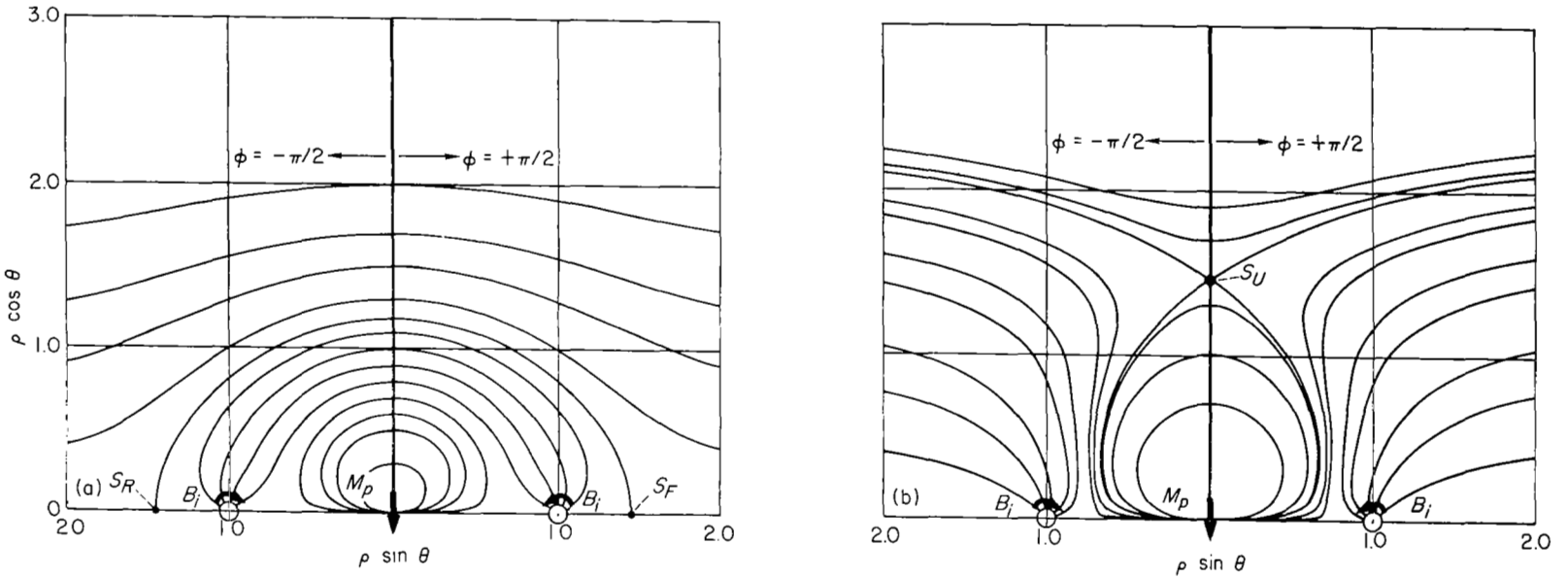

(a) Upper signs.
(b) Lower signs.

Figure 2.- Integral curves for equation (15) for $\alpha = 1$, $\mu = 1$, $\lambda = 0$.

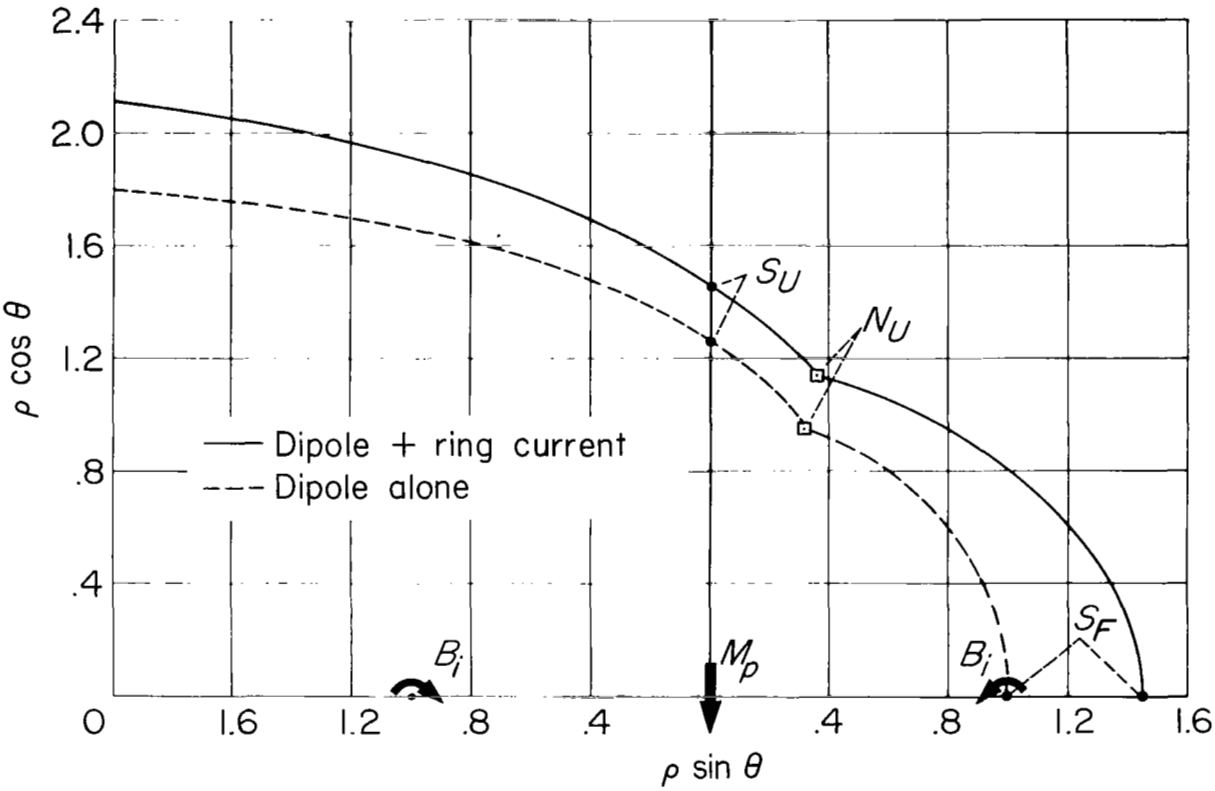

Figure 3.- Trace of the boundary of the geomagnetic field in the meridian plane. containing the dipole axis and the sun-earth line; $\alpha = 1$, $\mu = 1$, $\lambda = 0$.

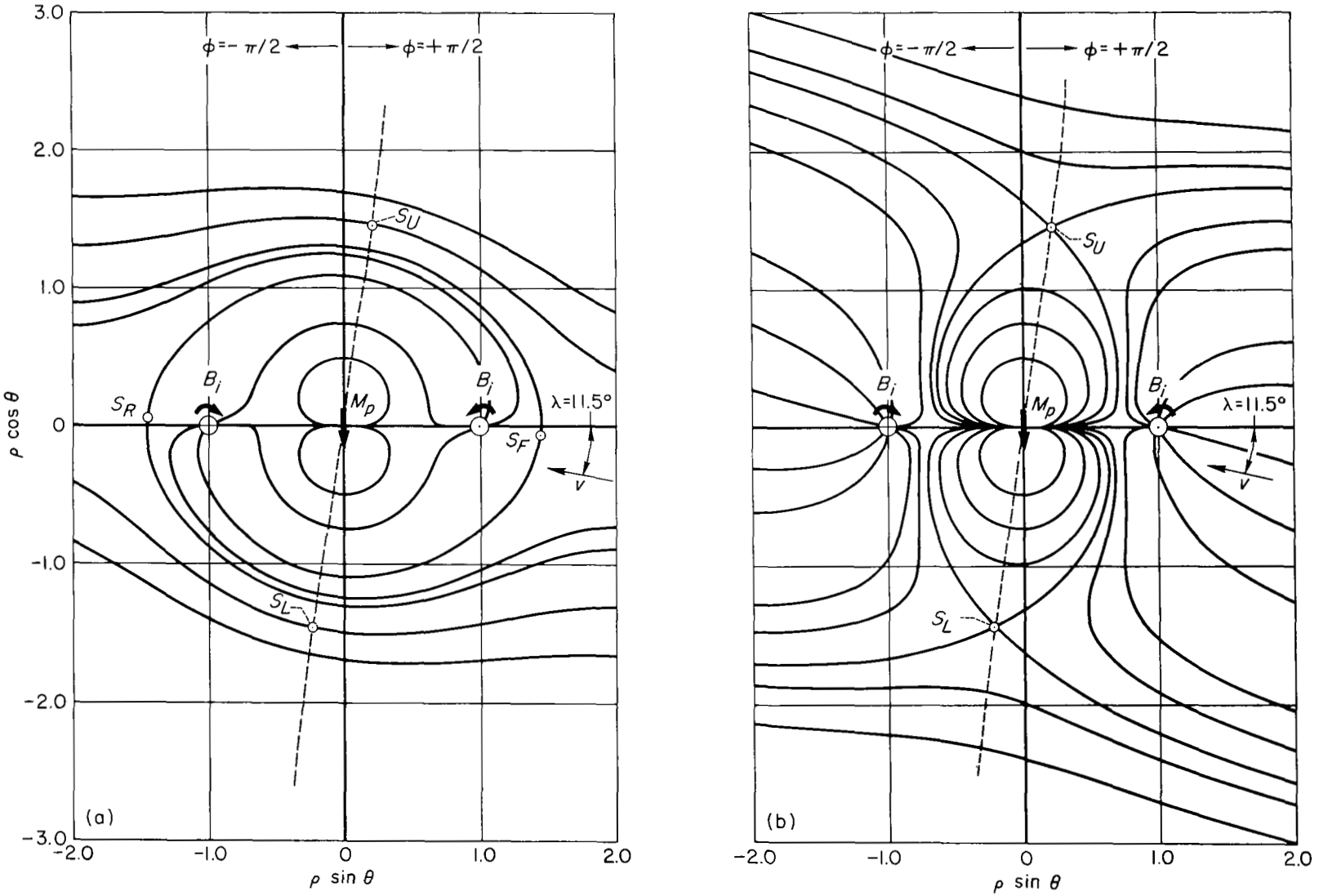

(a) Upper signs.
(b) Lower signs.

Figure 4.- Integral curves for equation (15) for $\alpha = 1$, $\mu = 1$, $\lambda = 11.5^{\circ}$.

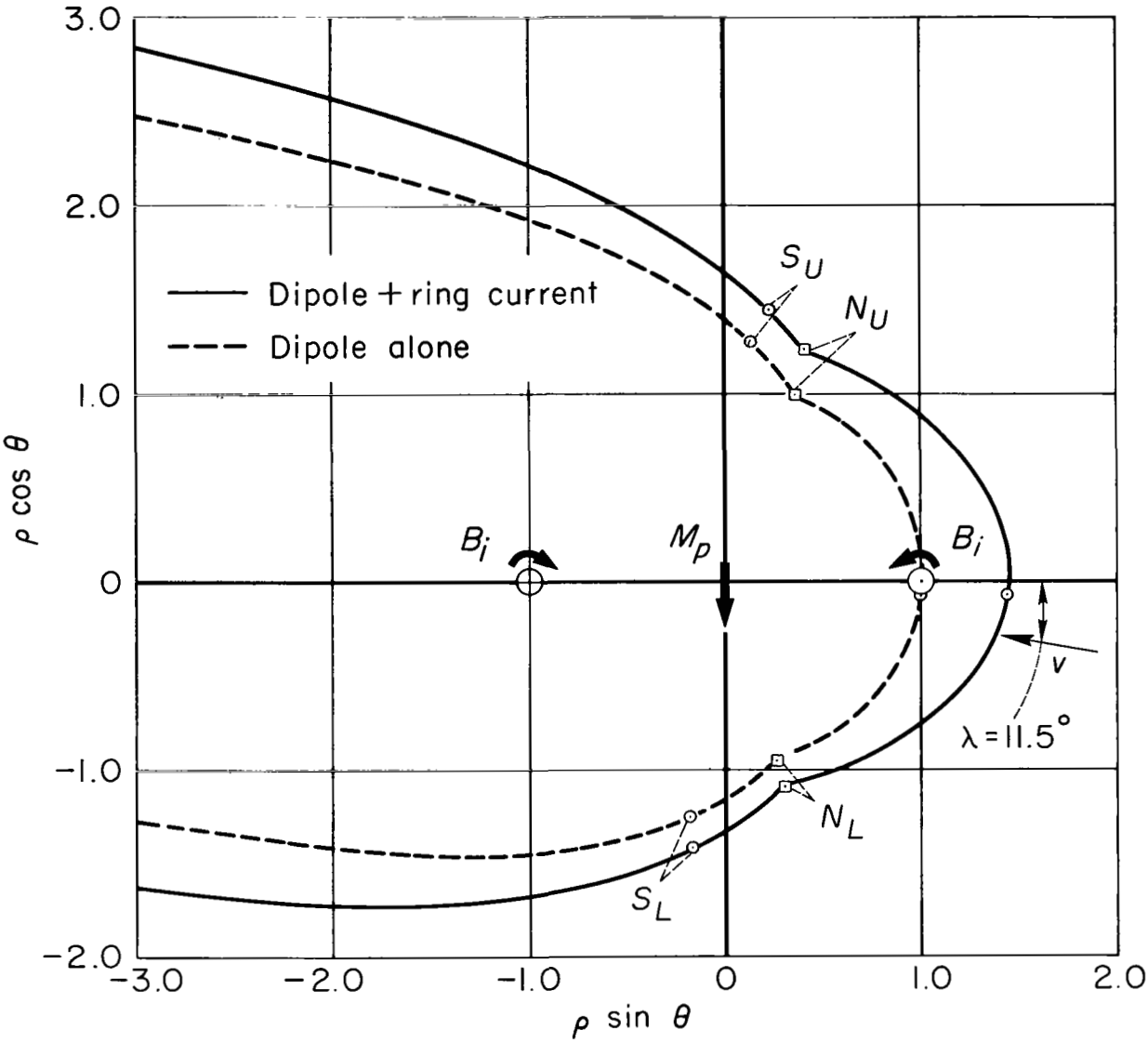

Figure 5.- Trace of the boundary of the geomagnetic field in the meridian plane containing the dipole axis and the sun-earth line; $\alpha = 1$, $\mu = 1$, $\lambda = 11.5^{\circ}$.

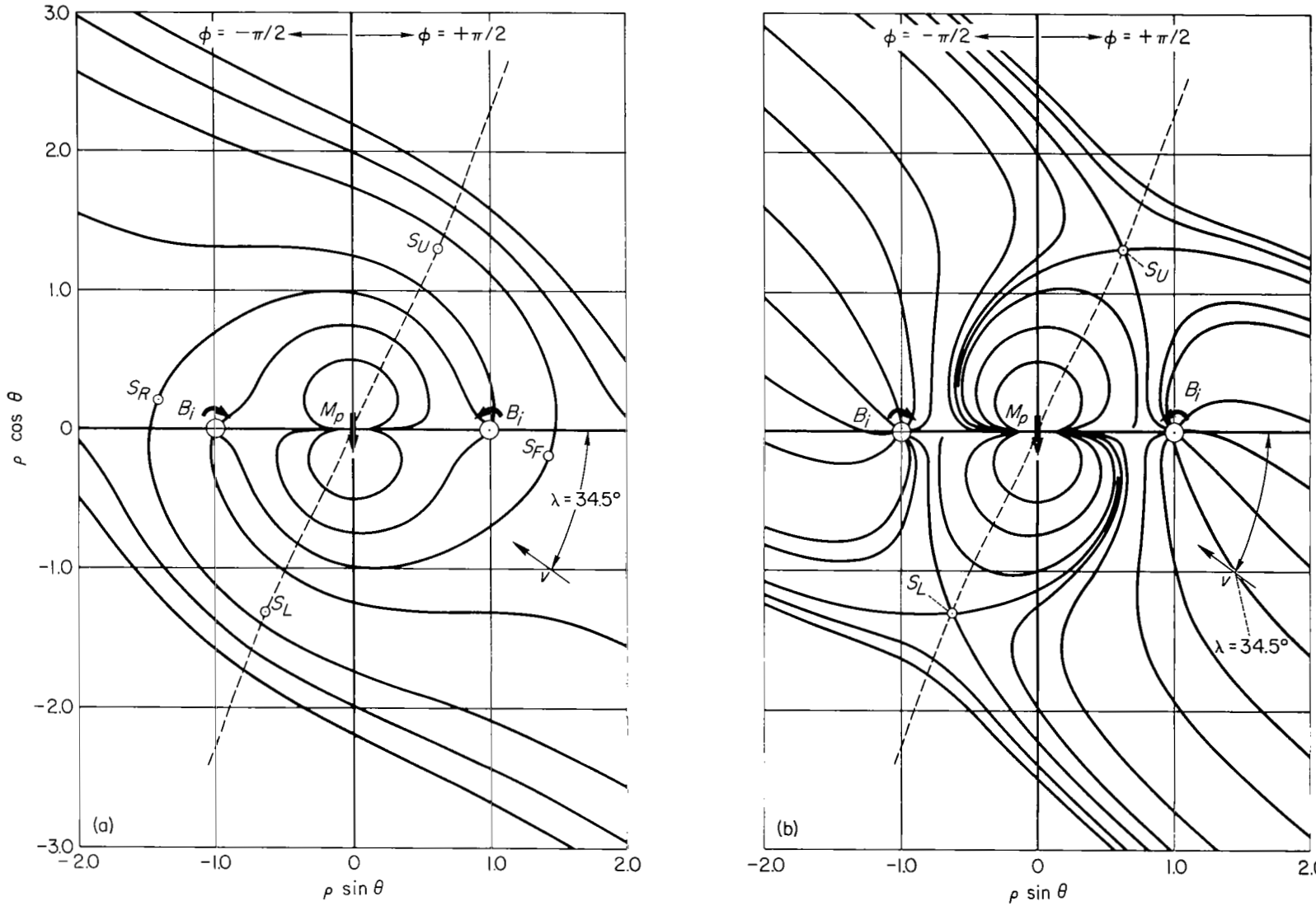

(a) Upper signs.
(b) Lower signs.

Figure 6.- Integral curves for equation (15) for $\alpha = 1$, $\mu = 1$, $\lambda = 34.5^{\circ}$.

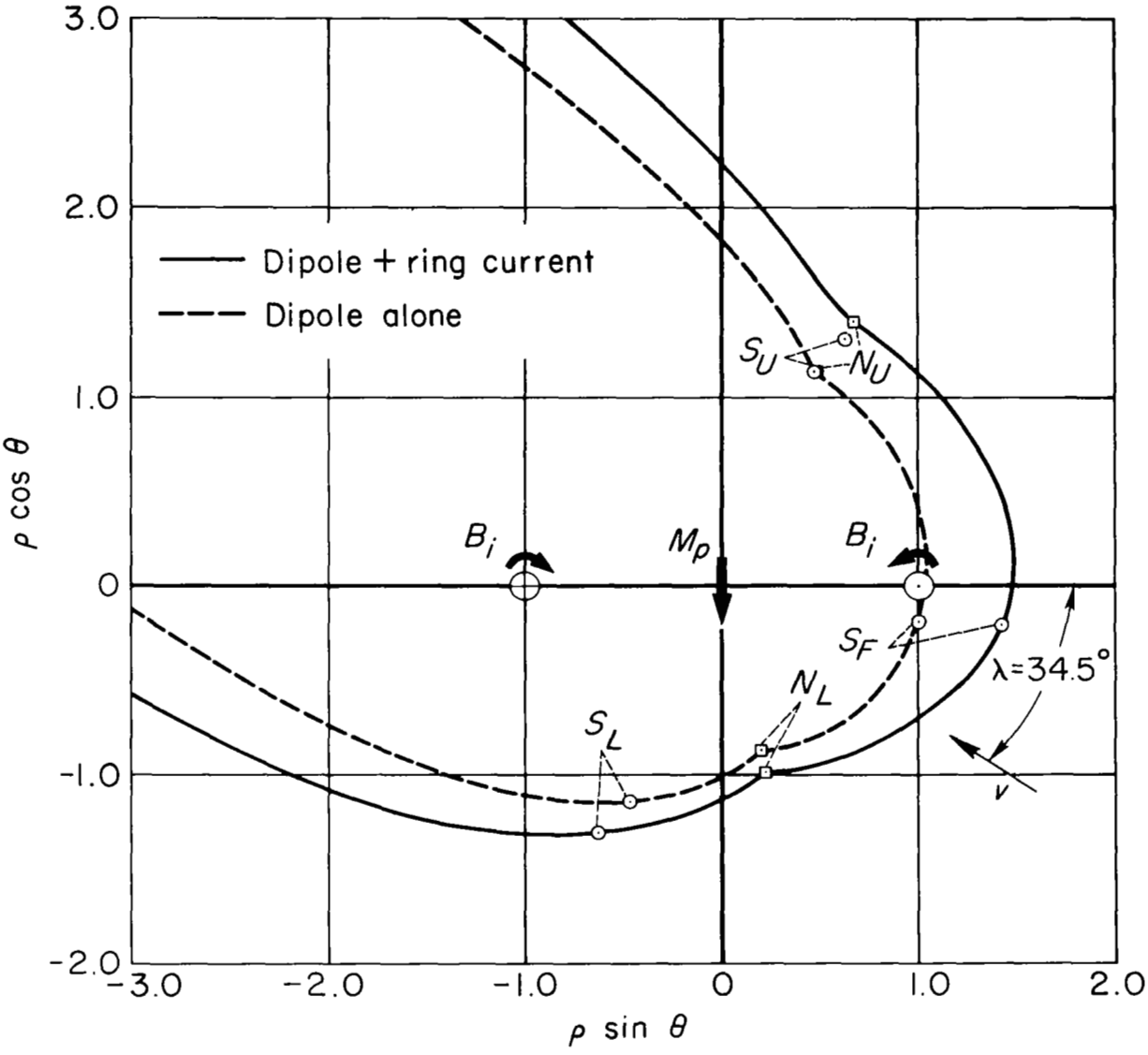

Figure 7.- Trace of the boundary of the geomagnetic field in the meridian plane containing the dipole axis and the sun-earth line; $\alpha = 1$, $\mu = 1$, $\lambda = 34.5^{\circ}$.

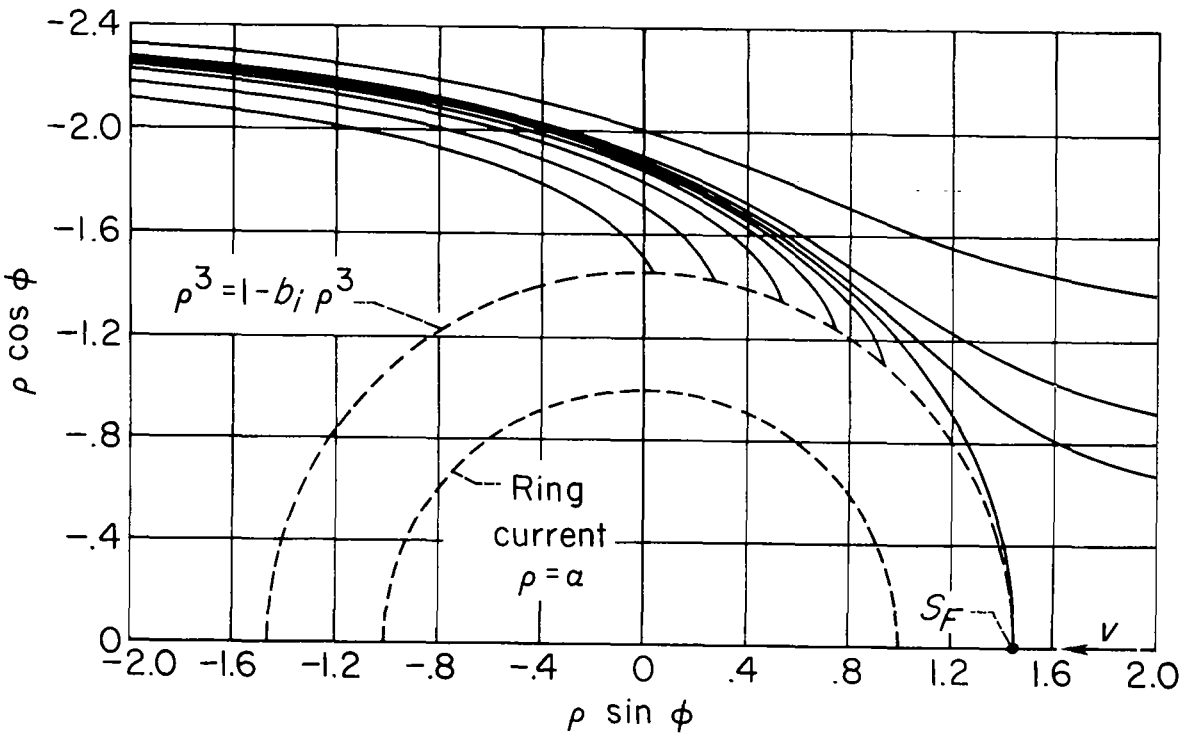

Figure 8.- Integral curves for equation (20) for $\alpha = 1$, $\mu = 1$.

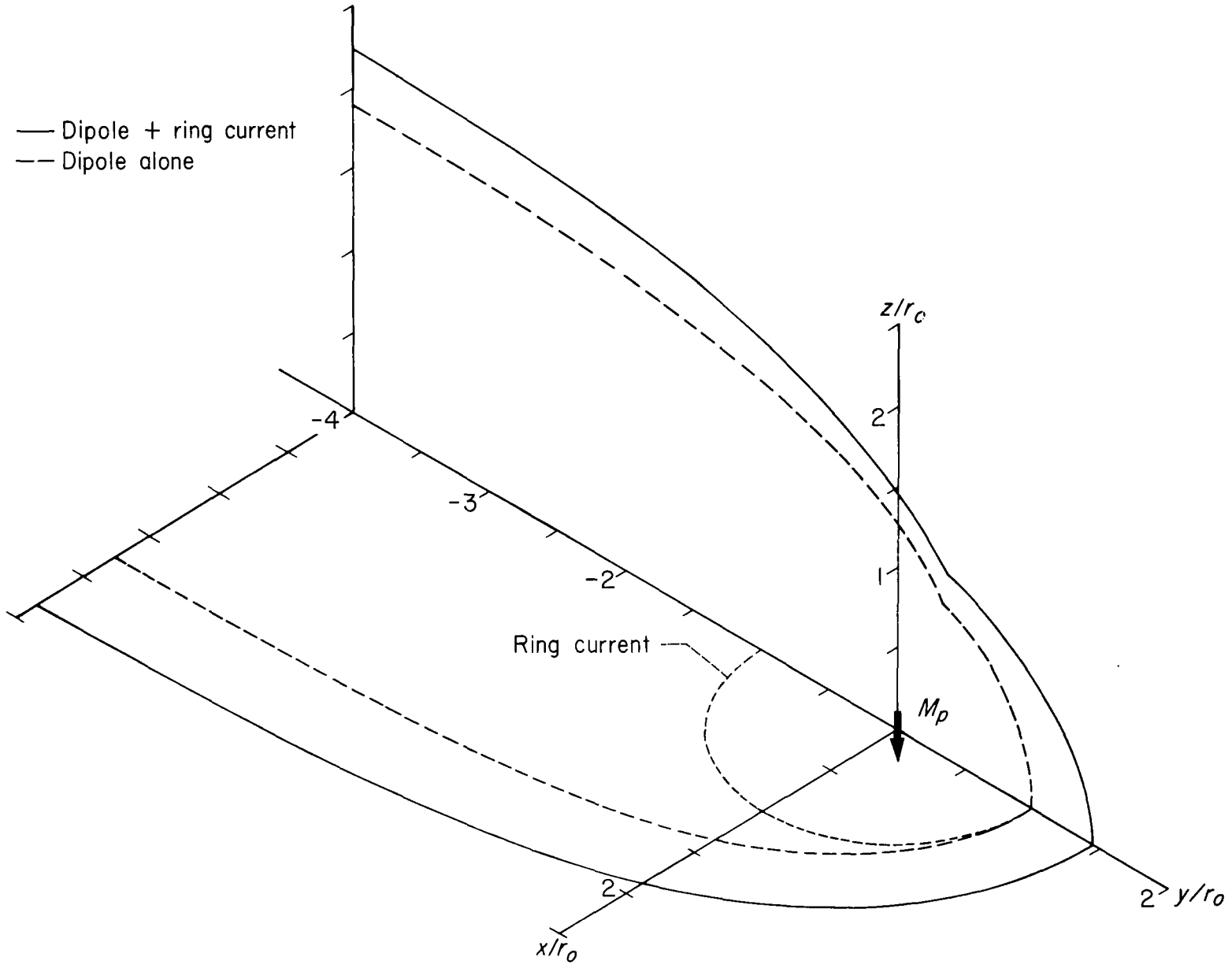

Figure 9.- Traces of the boundary of the geomagnetic field in the equatorial plane and in the meridian plane containing the dipole axis and the sun-earth line, $\alpha = 1$, $\mu = 1$, $\lambda = 0$.

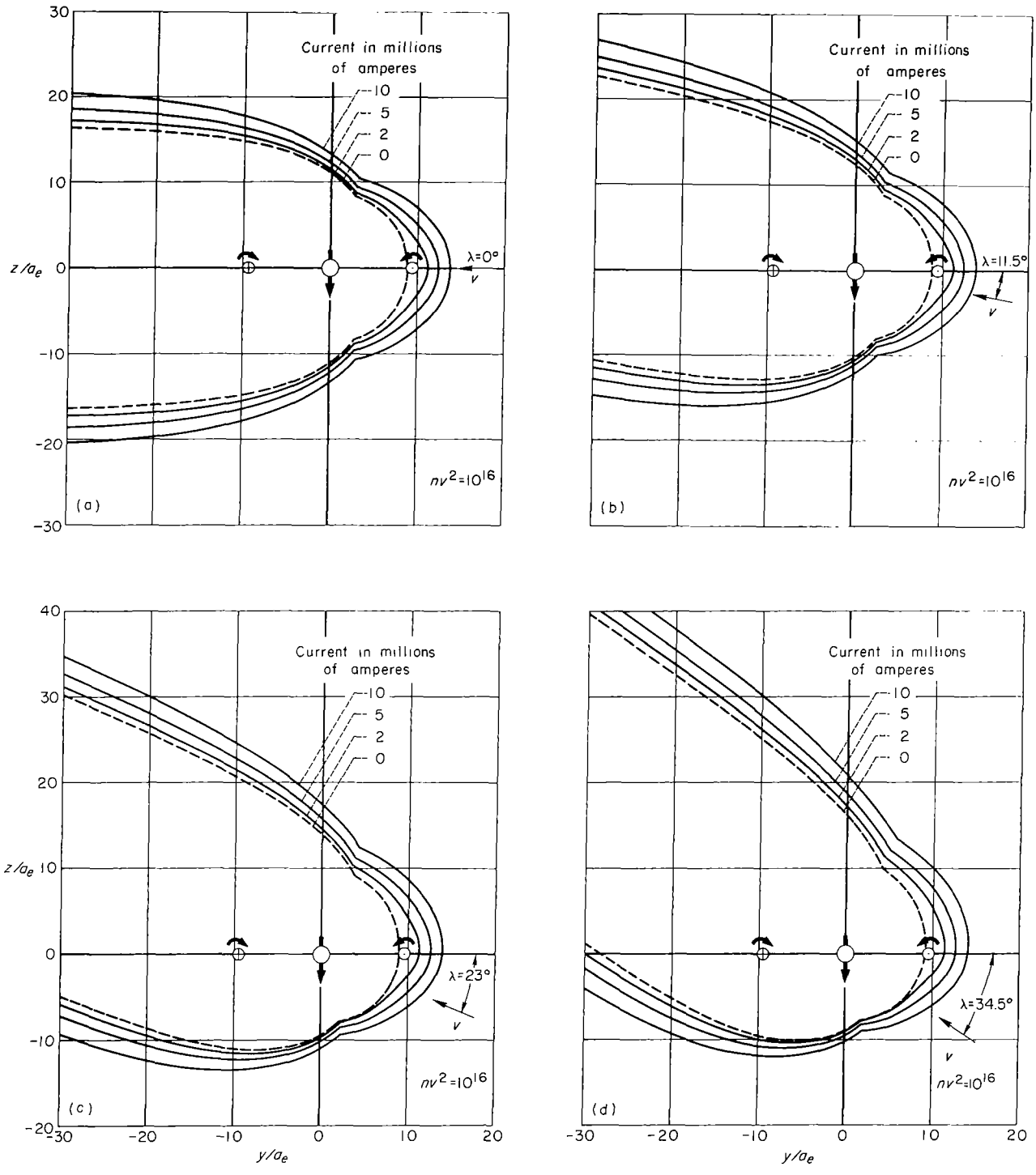

Figure 10.- Traces of the boundary of the geomagnetic field in the meridian plane containing the dipole axis and the sun-earth line for various strengths of the ring current; $nv^2 = 10^{16}$ protons/cm sec^2, a = 6×10^9 cm = 60,000 km.

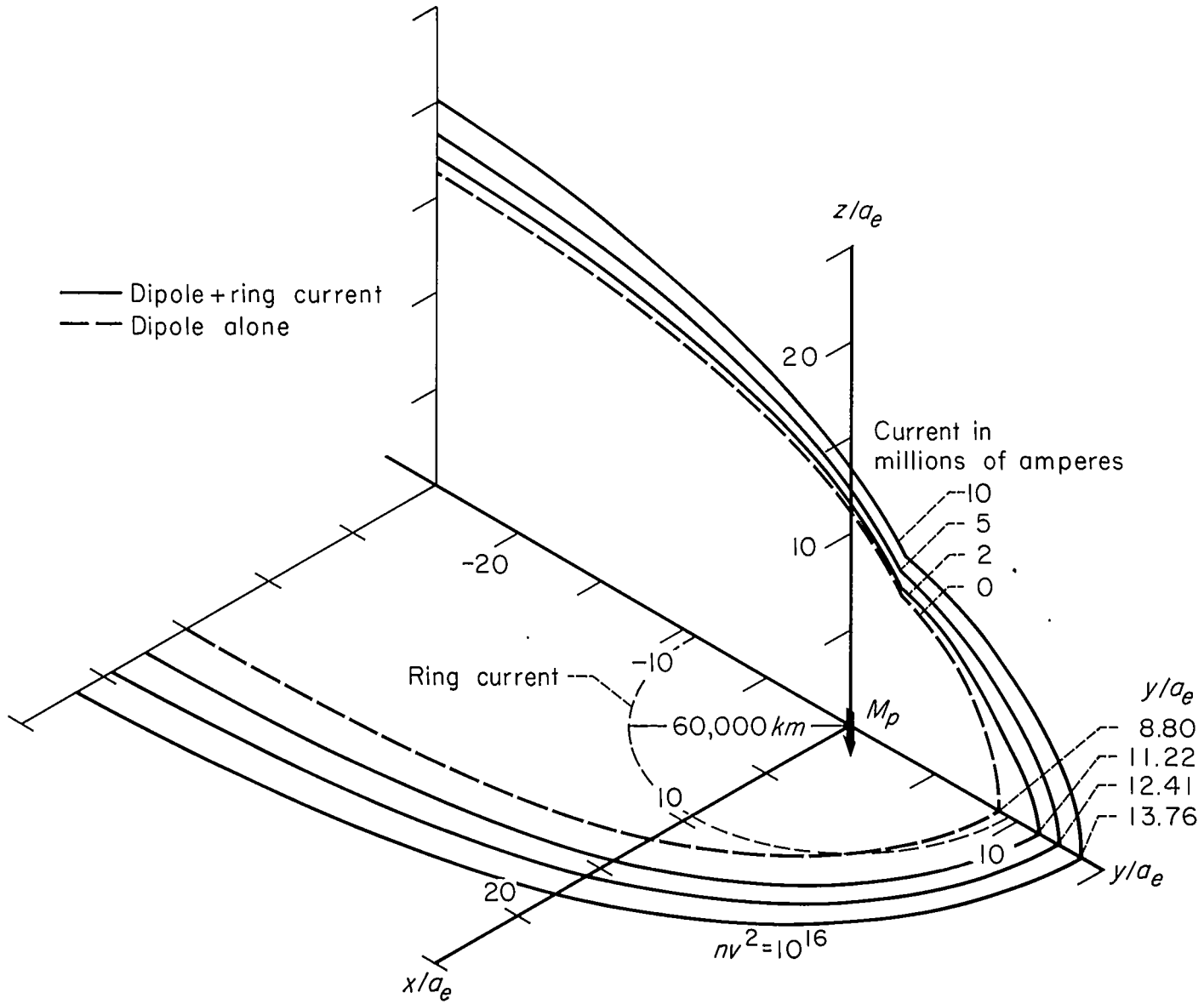

Figure 11.- Traces of the boundary of the geomagnetic field in the equatorial plane and in the meridian plane containing the dipole axis and the sun-earth line for various strengths of the ring current; $nv^2 = 10^{16}$ protons/cm sec^2, $a = 6 \times 10^9$ cm = 60,000 km, $\lambda = 0$.

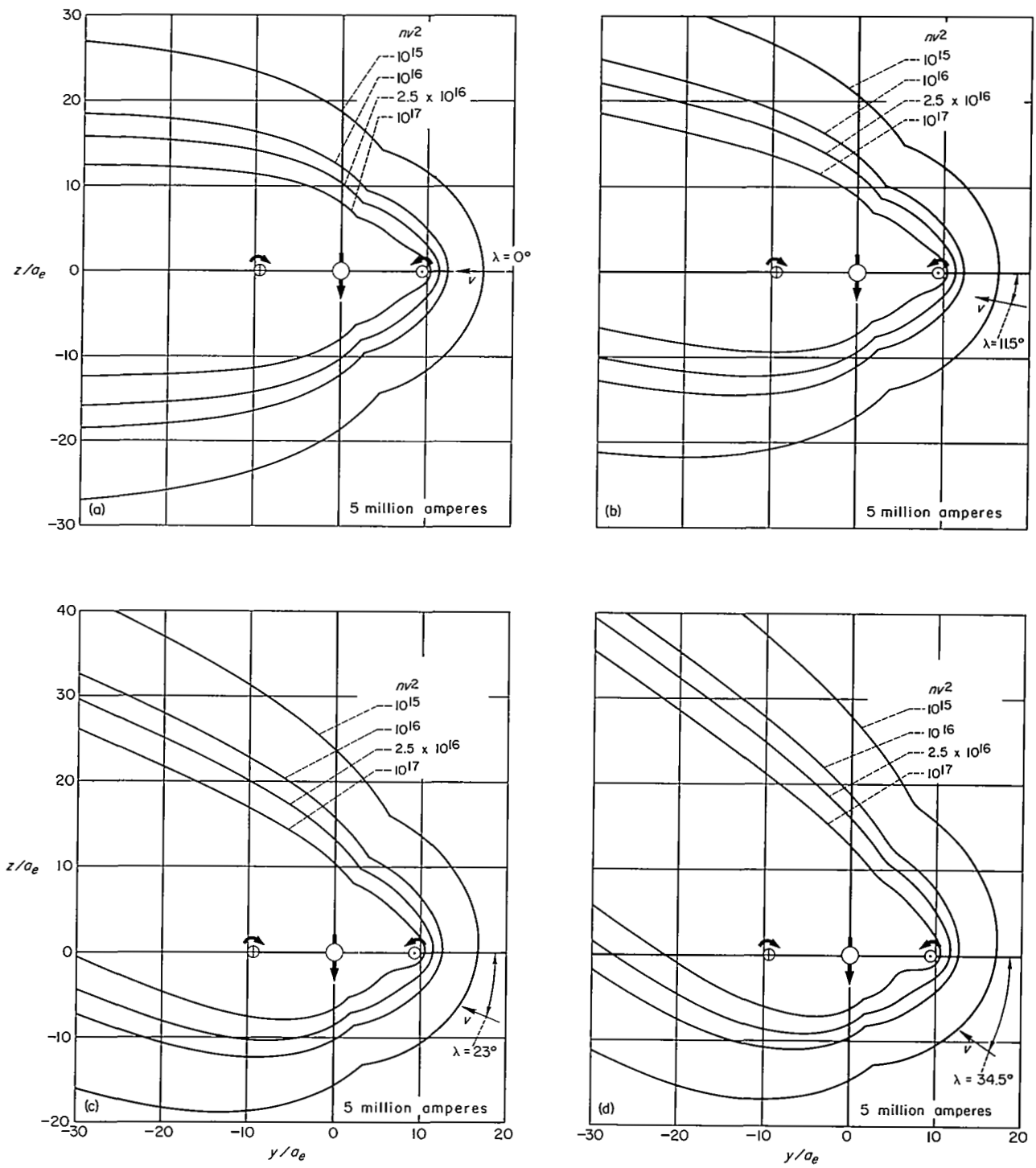

Figure 12.- Traces of the boundary of the geomagnetic field in the meridian plane containing the dipole axis and the sun-earth line for various intensities of the solar wind; a = 6×10^9 cm = 60,000 km, i = 5×10^5 e.m.u. = 5 million amperes.

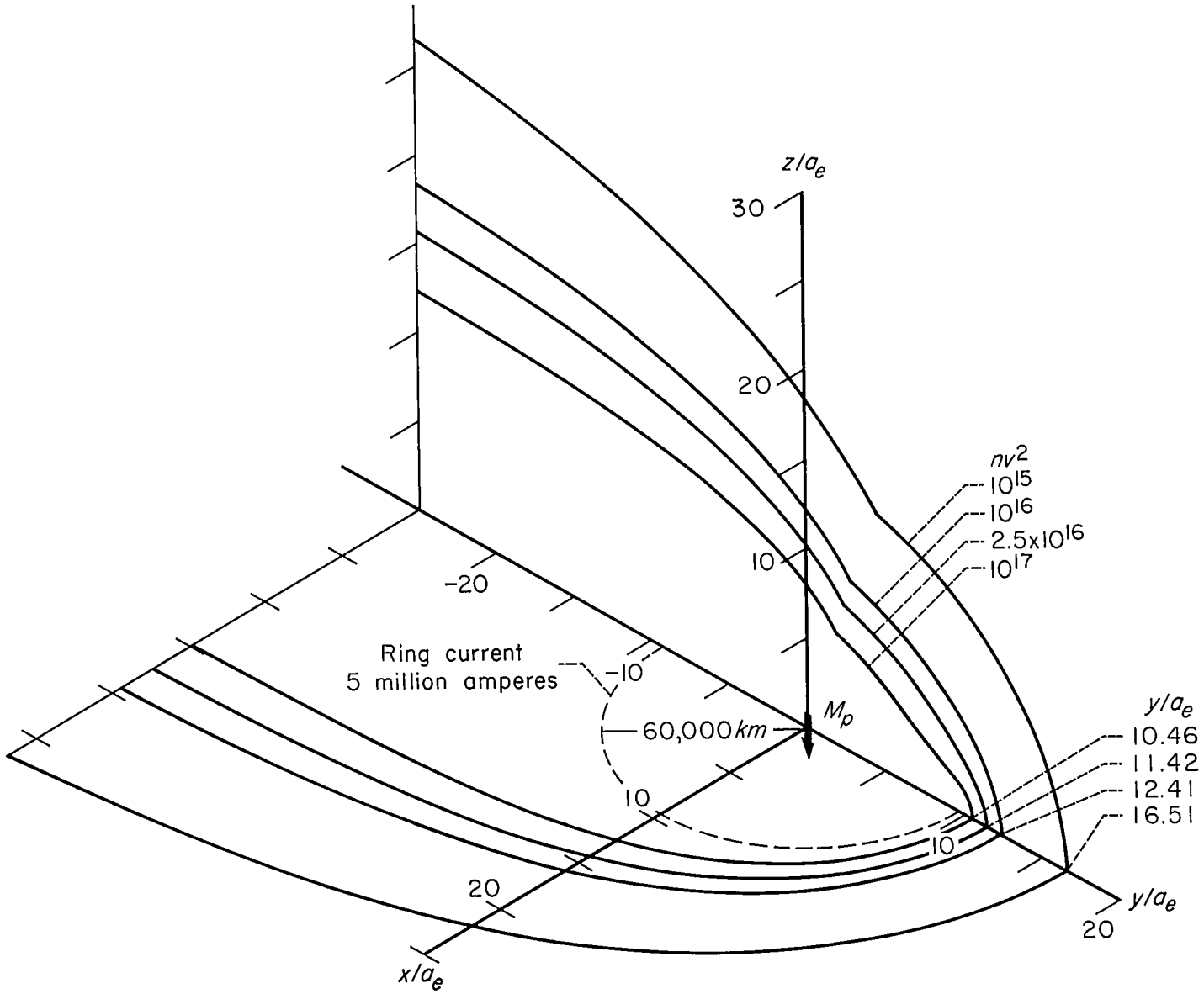

Figure 13.- Traces of the boundary of the geomagnetic field in the equatorial plane and in the meridian plane containing the dipole axis and the sun-earth line for various strengths of the ring current; $nv^2 = 10^{16}$ protons/cm sec^2, $a = 6\times10^9$ cm = 60,000 km, $\lambda = 0$.

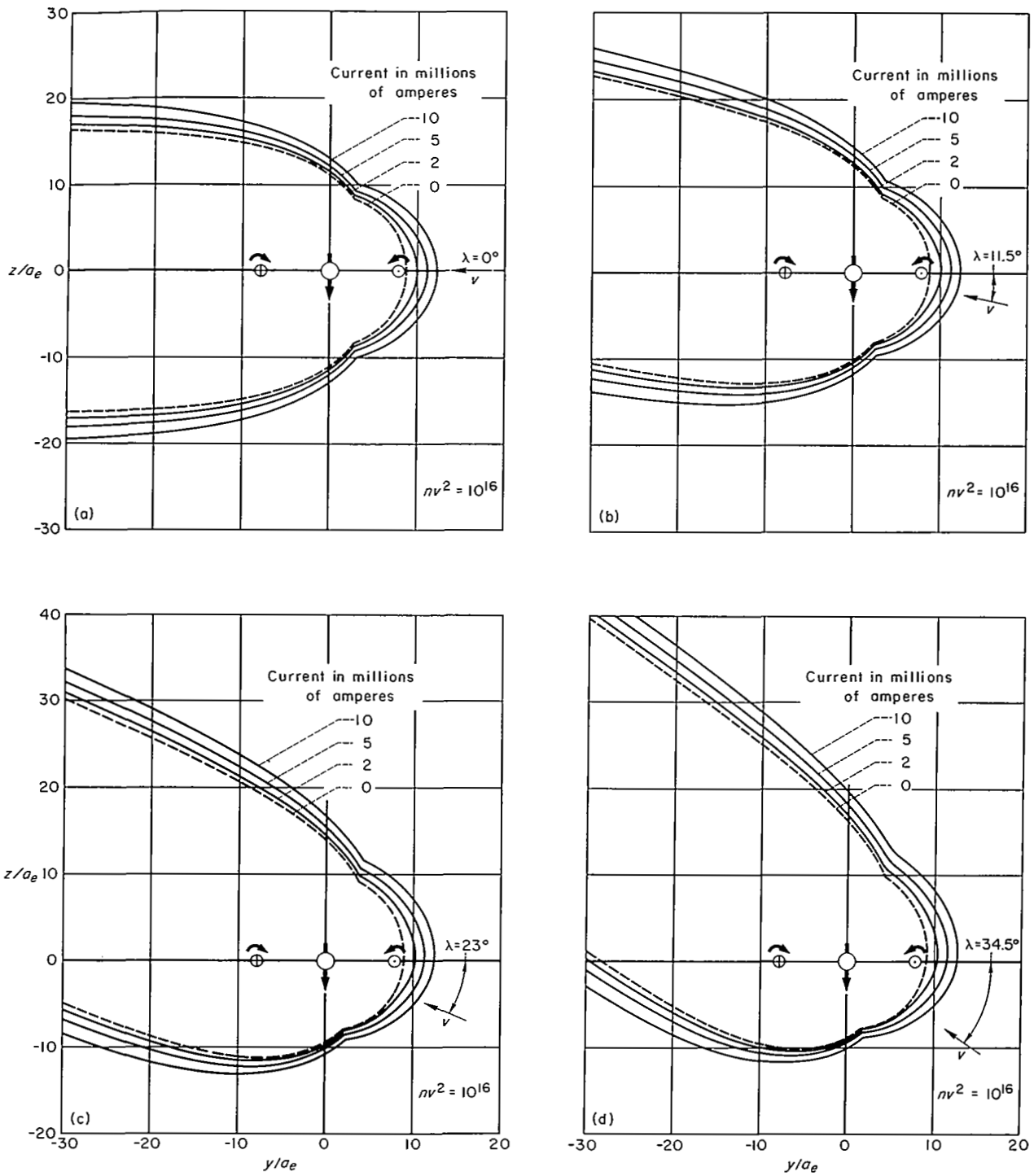

Figure 14.- Traces of the boundary of the geomagnetic field in the meridian plane containing the dipole axis and the sun-earth line for various strengths of the ring current; $nv^2 = 10^{16}$ protons/cm sec^2, a = 5×10^9 cm = 50,000 km.

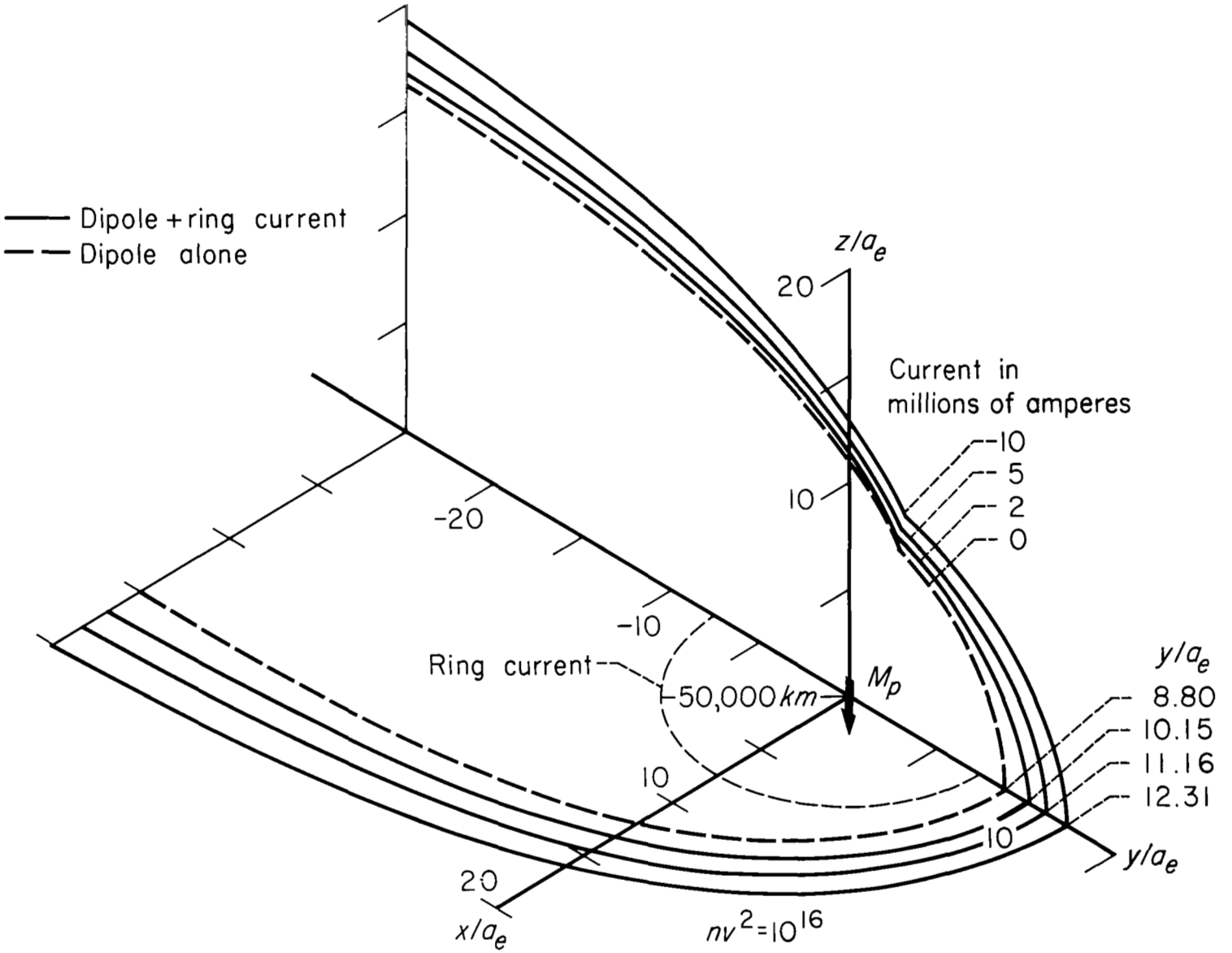

Figure 15.- Traces of the boundary of the geomagnetic field in the equatorial plane and in the meridian plane containing the dipole axis and the sun-earth line for various strengths of the ring current; $nv^2 = 10^{16}$ protons/cm sec^2, a = 5×10^9 cm = 50,000 km, $\lambda = 0$.

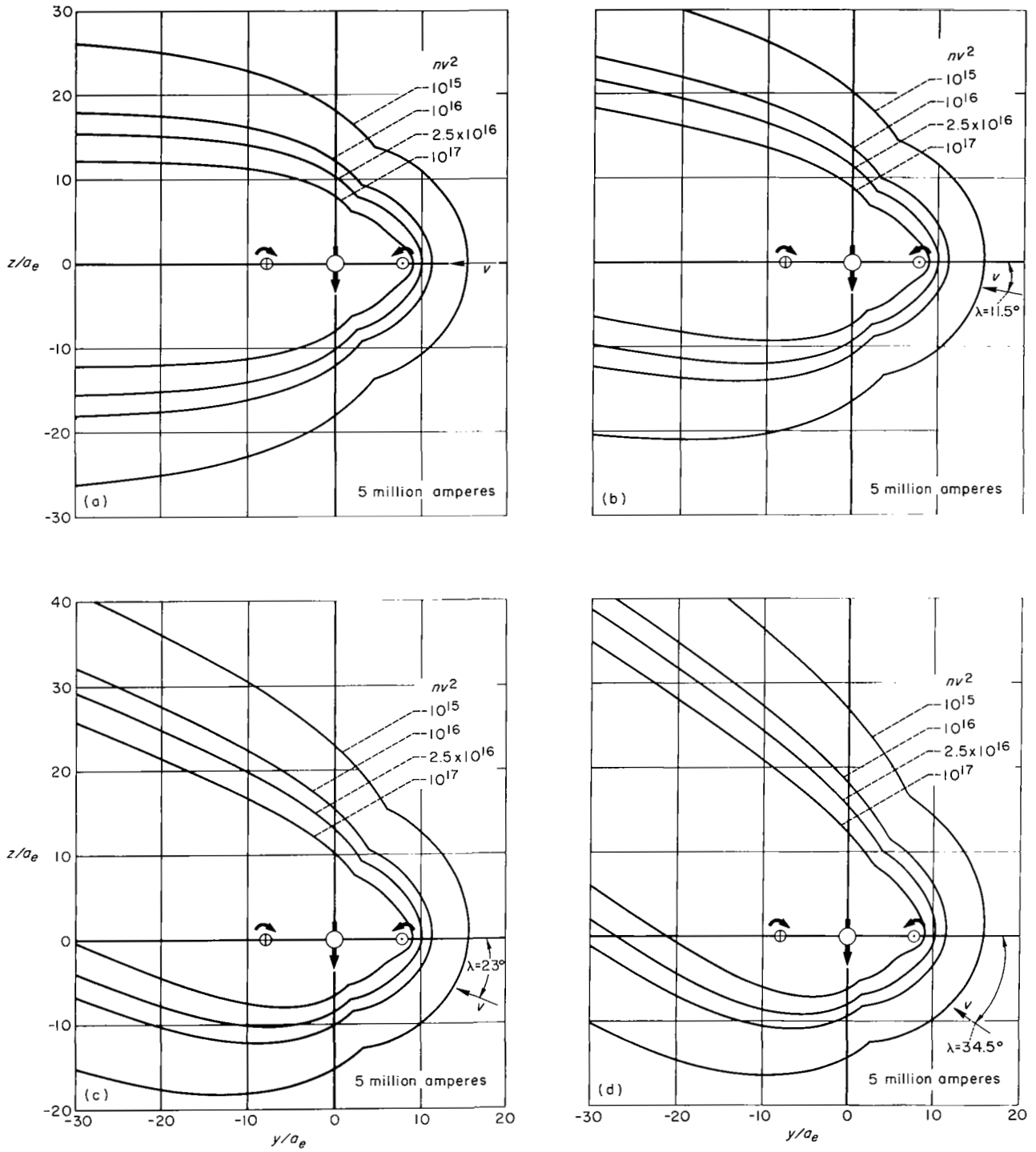

Figure 16.- Traces of the boundary of the geomagnetic field in the meridian plane containing the dipole axis and the sun-earth line for various intensities of the solar wind; a = 5×10^9 cm = 50,000 km, i = 5×10^5 e.m.u. = 5 million amperes.

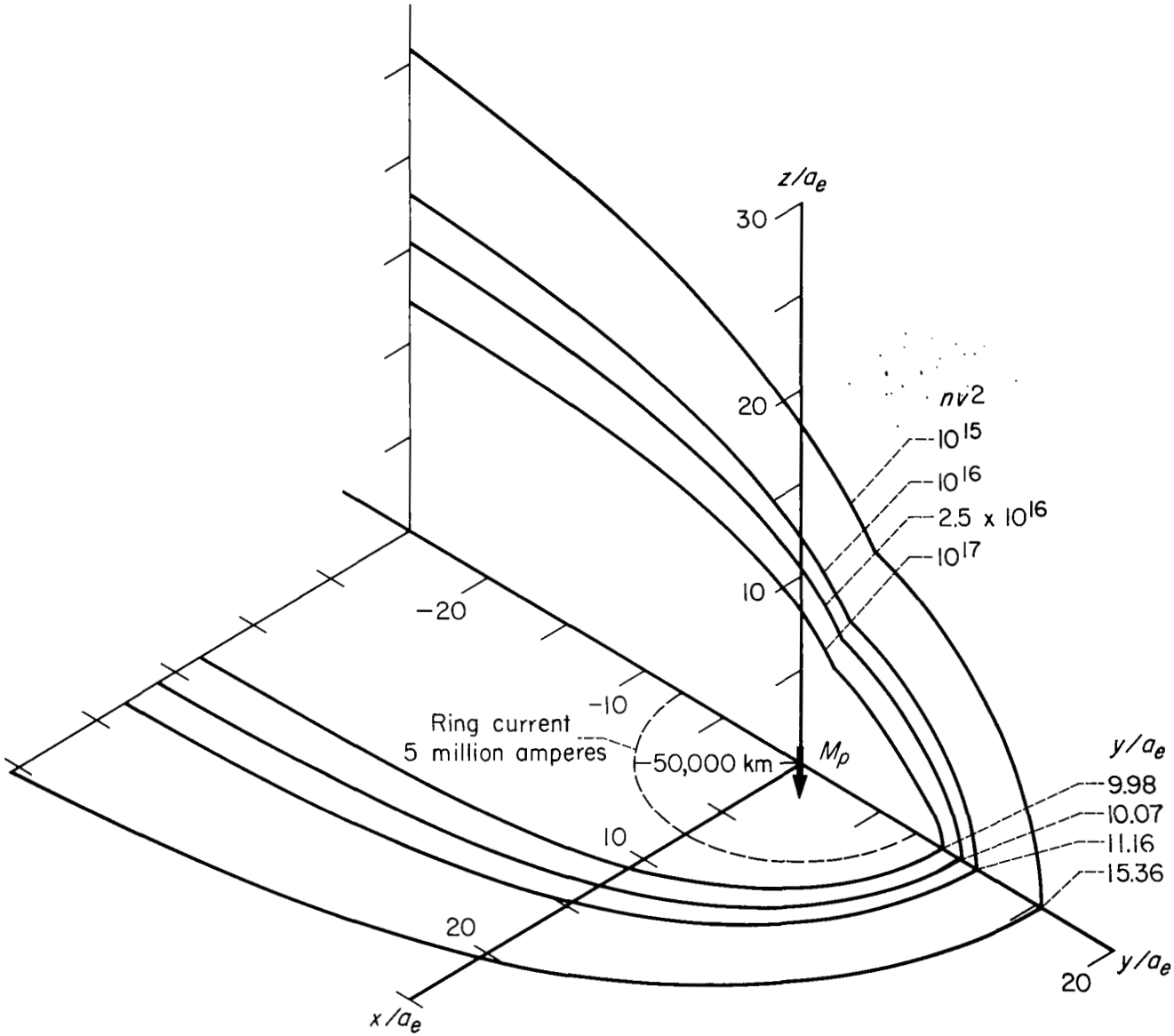

Figure 17.- Traces of the boundary of the geomagnetic field in the equatorial plane and in the meridian plane containing the dipole axis and the sun-earth line for various intensities of the solar wind; $a = 5 \times 10^9$ cm = 50,000 km, $i = 5 \times 10^5$ e.m.u. = 5 million amperes, $\lambda = 0$.

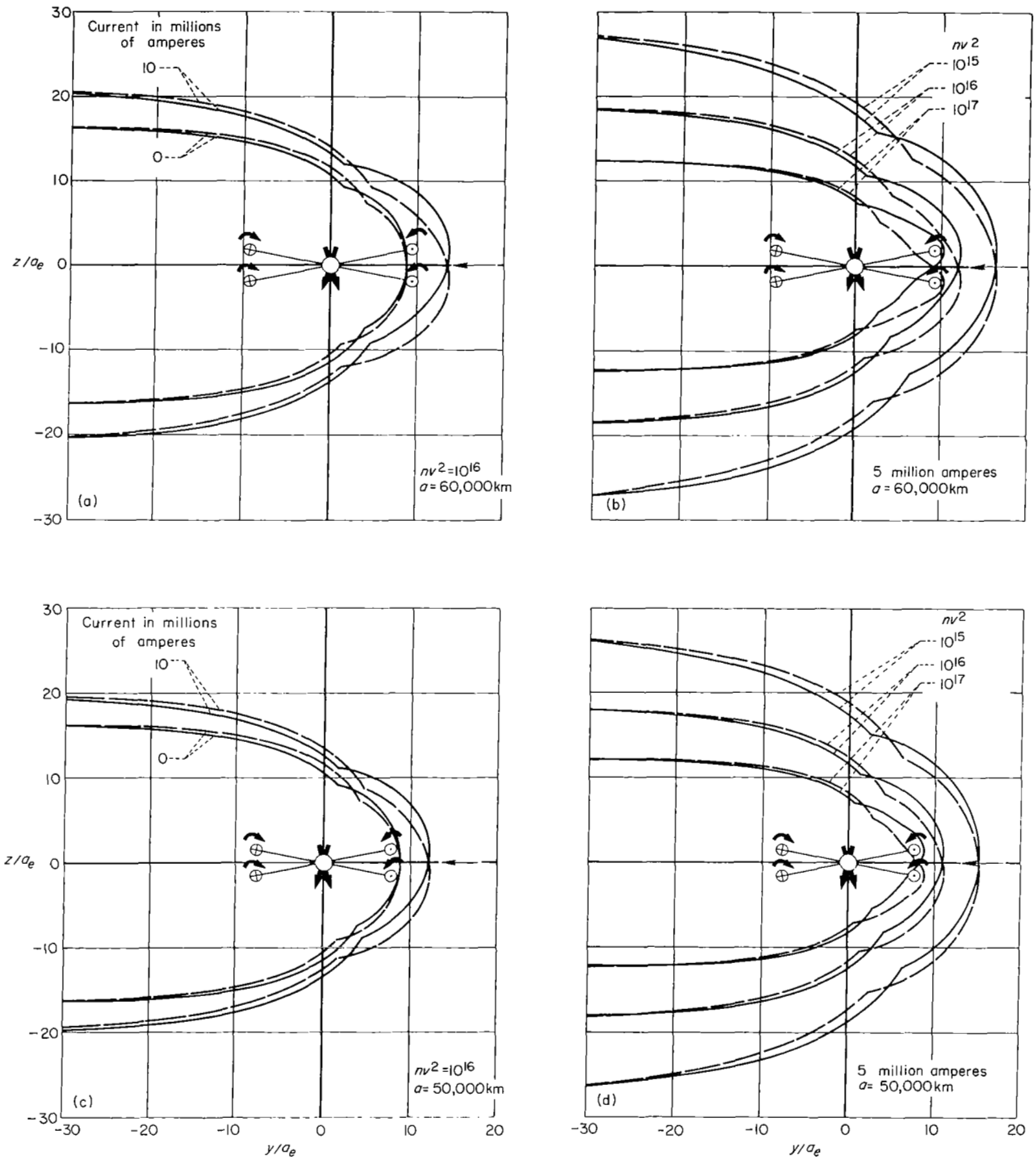

Figure 18.- Traces of the boundary of the geomagnetic field in the meridian plane containing the dipole axis and the sun-earth line illustrated in coordinates fixed with respect to the solar wind; $\lambda = \pm 11.5^{\circ}$.

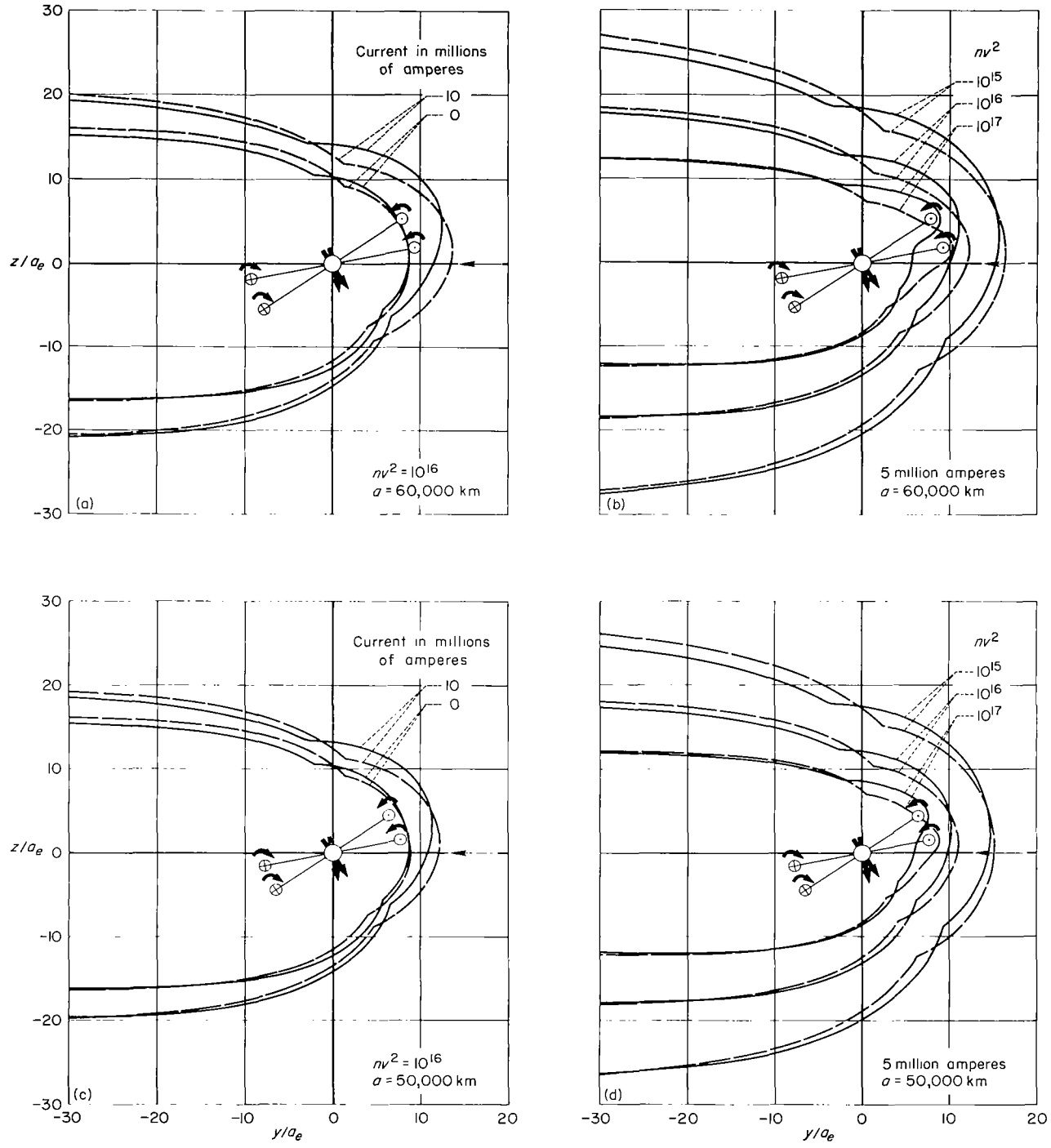

Figure 19.- Traces of the boundary of the geomagnetic field in the meridian plane containing the dipole axis and the sun-earth line illustrated in coordinates fixed with respect to the solar wind; $\lambda = 11.5^{\circ}$ and 34.5°.

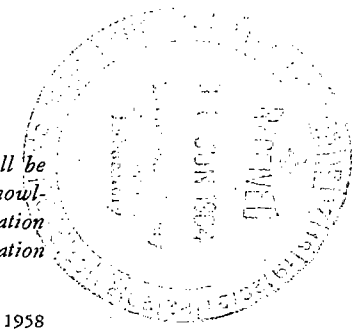

"The aeronautical and space activities of the United States shall be conducted so as to contribute . . . to the expansion of human knowledge of phenomena in the atmosphere and space. The Administration shall provide for the widest practicable and appropriate dissemination of information concerning its activities and the results thereof."

—NATIONAL AERONAUTICS AND SPACE ACT OF 1958

NASA SCIENTIFIC AND TECHNICAL PUBLICATIONS

TECHNICAL REPORTS: Scientific and technical information considered important, complete, and a lasting contribution to existing knowledge.

TECHNICAL NOTES: Information less broad in scope but nevertheless of importance as a contribution to existing knowledge.

TECHNICAL MEMORANDUMS: Information receiving limited distribution because of preliminary data, security classification, or other reasons.

CONTRACTOR REPORTS: Technical information generated in connection with a NASA contract or grant and released under NASA auspices.

TECHNICAL TRANSLATIONS: Information published in a foreign language considered to merit NASA distribution in English.

TECHNICAL REPRINTS: Information derived from NASA activities and initially published in the form of journal articles.

SPECIAL PUBLICATIONS: Information derived from or of value to NASA activities but not necessarily reporting the results of individual NASA-programmed scientific efforts. Publications include conference proceedings, monographs, data compilations, handbooks, sourcebooks, and special bibliographies.

Details on the availability of these publications may be obtained from:

SCIENTIFIC AND TECHNICAL INFORMATION DIVISION

NATIONAL AERONAUTICS AND SPACE ADMINISTRATION

Washington, D.C. 20546